© 2021. Published by The Company of Biologists Ltd | Journal of Cell Science (2021) 135, jcs258671. doi:10.1242/jcs.258671

RESEARCH ARTICLE

Ca^{2+} release via $InsP_3Rs$ enhances RyR recruitment during Ca^{2+} transients by increasing dyadic [Ca^{2+}] in cardiomyocytes

Kateryna Demydenko, Karin R. Sipido and H. Llewelyn Roderick*

ABSTRACT

Excitation–contraction coupling (ECC) relies on temporally synchronized sarcoplasmic reticulum (SR) Ca^{2+} release via ryanodine receptors (RyRs) at dyadic membrane compartments. Neurohormones, such as endothelin-1 (ET-1), that act via $G\alpha_q$-associated G protein-coupled receptors (GPCRs) modulate Ca^{2+} dynamics during ECC and induce SR Ca^{2+} release events involving Ca^{2+} release via inositol 1,4,5-trisphosphate ($InsP_3$) receptors ($InsP_3Rs$). How the relatively modest Ca^{2+} release via $InsP_3Rs$ elicits this action is not resolved. Here, we investigated whether the actions of $InsP_3Rs$ on Ca^{2+} handling during ECC were mediated by a direct influence on dyadic Ca^{2+} levels and whether this mechanism contributes to the effects of ET-1. Using a dyad-targeted genetically encoded Ca^{2+} reporter, we found that $InsP_3R$ activation augmented dyadic Ca^{2+} fluxes during Ca^{2+} transients and increased Ca^{2+} sparks. RyRs were required for these effects. These data provide the first direct demonstration of GPCR and $InsP_3$ effects on dyadic Ca^{2+}, and support the notion that Ca^{2+} release via $InsP_3Rs$ influences Ca^{2+} transients during ECC by facilitating the activation and recruitment of proximal RyRs. We propose that this mechanism contributes to neurohormonal modulation of cardiac function.

This article has an associated First Person interview with the first author of the paper.

KEY WORDS: Cardiac excitation–contraction coupling, $InsP_3R$, RyR, Ca^{2+} microdomains, Ca^{2+} release, Ca^{2+} sparks, Ca^{2+} nanosparks

INTRODUCTION

The contraction of cardiomyocytes required for the pumping action of the heart is brought about via excitation–contraction coupling (ECC) (Bers, 2002; Gilbert et al., 2020). Underlying this process is the action potential-mediated opening of voltage-gated L-type Ca^{2+} channels (LTCCs) on the sarcolemma, which evokes a brief Ca^{2+} influx into the cell that is amplified by ryanodine receptors (RyRs) on the sarcoplasmic reticulum (SR). This process of Ca^{2+}-induced Ca^{2+} release (CICR) occurs in cellular microdomains termed dyads that are formed by juxtaposition of LTCCs in the sarcolemma and RyRs in the SR within a narrow 12–15 nm junctional cleft (Sun et al., 1995). In ventricular cardiomyocytes, due to T-tubular invaginations of sarcolemma (TTs), these release sites are distributed across the entire volume of the cardiomyocyte, thereby facilitating a synchronized and cell-wide release of Ca^{2+} from the SR during cell depolarization (Brette and Orchard, 2003).

Through alteration of Ca^{2+} dynamics, circulating and local mediators regulate the strength of cardiomyocyte contraction to meet hemodynamic needs. Although catecholamines play a pivotal role in this process, other autocrine/paracrine hormones, including endothelin-1 (ET-1) and angiotensin II (Ang II) also contribute (Mayourian et al., 2018). Under disease conditions, where their circulating levels are often increased, these mediators contribute to pathology, for example stimulation of pro-arrhythmic activity, including induction of spontaneous Ca^{2+} release events (Hiroe et al., 1991; McMurray et al., 1992; Signore et al., 2013; Stewart et al., 1992; Van De Wal et al., 2006; Yorikane et al., 1993).

Inositol 1,4,5-trisphosphate ($InsP_3$)-induced Ca^{2+} release (IICR) via SR-localized $InsP_3$ receptors ($InsP_3R$) contributes to the effects of $G\alpha_q$-associated G protein-coupled receptor (GPCR) activation on cardiomyocyte Ca^{2+} handling. GPCR engagement produces an increase in intracellular $InsP_3$ via phospholipase C-dependent hydrolysis of phosphatidyl inositol 4,5-bisphosphate (Drawnel et al., 2013). Although expression of $InsP_3R$ (predominantly the type 2 isoform, $InsP_3R2$, also known as ITPR2) in the heart of various mammalian species is well described, the interactions between IICR and ECC are less consistent, particularly in healthy cardiomyocytes, and shows variation between species (Blanch i Salvador and Egger, 2018; Domeier et al., 2008; Harzheim et al., 2010, 2009; Ljubojevic et al., 2014; Proven et al., 2006; Signore et al., 2013; Smyrnias et al., 2018; Wu et al., 2006; Zima and Blatter, 2004). Indeed, while in rabbit, inotropic effects are observed (Domeier et al., 2008), IICR does not contribute to the inotropic action of ET-1 in rat (Harzheim et al., 2009; Smyrnias et al., 2018). Elsewhere, in human and mouse cardiomyocytes, GPCR/$InsP_3$/$InsP_3R$ axis activation augments pacing-evoked Ca^{2+} transients and cell contraction (Signore et al., 2013). While these effects of $InsP_3$ on healthy cardiomyocytes may be beneficial, the effects of $InsP_3R$ activation are amplified in disease contributing to pathological increases in spontaneous Ca^{2+} release events and to arrhythmogenic Ca^{2+} transients (Blanch i Salvador and Egger, 2018; Harzheim et al., 2009; Nakayama et al., 2010; Proven et al., 2006; Signore et al., 2013). These deleterious aspects of $InsP_3$ signaling arise due to an increase in expression of $InsP_3R$ and levels of GPCRs and their ligands that promote generation of $InsP_3$ (Go et al., 1995; Harzheim et al., 2010; Regitz-Zagrosek et al., 1995; Tsutsumi et al., 1998; Zolk et al., 1999).

Despite the lack of consistency in the effects of $InsP_3$ on Ca^{2+} transients between species and studies, a Ca^{2+}-mobilizing activity of $InsP_3$ is universally reported (Blanch i Salvador and Egger, 2018; Domeier et al., 2008; Harzheim et al., 2009; Horn et al., 2013). However, these specific actions of $InsP_3$ often require analysis in the absence of the bulk changes in Ca^{2+} associated with ECC, precluding a full understanding of the mechanism by which

KU Leuven, Department of Cardiovascular Sciences, Laboratory of Experimental Cardiology, B-3000, Leuven, Belgium.

*Author for correspondence (llewelyn.roderick@kuleuven.be)

H.L.R., 0000-0001-7065-3523

Handling Editor: John Heath
Received 24 March 2021; Accepted 8 June 2021

Journal of Cell Science (2021) 135, jcs258671. doi:10.1242/jcs.258671

IICR modulates ECC-associated Ca^{2+} transients. Under these conditions, the actions of $InsP_3$ are manifested as an increase in Ca^{2+} sparks and/or a depletion of the SR Ca^{2+} store (Blanch i Salvador and Egger, 2018; Domeier et al., 2008; Harzheim et al., 2009; Horn et al., 2013; Wullschleger et al., 2017; Zima and Blatter, 2004). Notably, RyRs are in general required for this activity of $InsP_3$ to be fully manifested. Together, these data indicate that $InsP_3Rs$ are functionally expressed in cardiomyocytes and that the flux of Ca^{2+} via these receptors is small relative to RyRs. Based on these studies, we and others have proposed that despite their minor capacity to mobilize Ca^{2+} by themselves, through signaling crosstalk with RyRs, $InsP_3Rs$ acquire the capacity to influence ECC, including stimulation of pro-arrhythmic activity (Domeier et al., 2008; Harzheim et al., 2009; Wullschleger et al., 2017).

While dyadic colocalization of $InsP_3Rs$ and RyRs has been reported, enabling inter channel crosstalk (Harzheim et al., 2009), $InsP_3Rs$ have also been suggested to reside on regions of the SR distinct from those occupied by RyRs (Bare et al., 2005; Ljubojevic et al., 2014; Mohler et al., 2005). Although both scenarios could allow for $InsP_3R$–RyR signaling crosstalk, by generating a greater increase in Ca^{2+} local to the RyR, colocalization of $InsP_3Rs$ with RyRs in the dyad would be significantly more effective in promoting channel crosstalk. This could occur either through a direct activation via CICR or by bringing RyRs closer to threshold for activation by Ca^{2+} arising from voltage-gated Ca^{2+} channels and/or from Ca^{2+} arising from neighboring RyRs. Functional evidence supporting a role for IICR in modulation of dyadic RyR and Ca^{2+} dynamics is, however, lacking.

In this study, we therefore tested the hypothesis that IICR elicits its effects on Ca^{2+} transients through elevating dyadic Ca^{2+}, thereby either facilitating recruitment of RyRs or by enhancing Ca^{2+} fluxes via RyR clusters. To address these questions, we deployed a recently described dyad-targeted genetically encoded Ca^{2+} reporter GCaMP6f–triadin (targeted to the dyad by fusion with triadin) (Shang et al., 2014). In contrast to techniques employing inorganic dyes, this reporter allows the direct measurement of Ca^{2+} dynamics during ECC in intact cardiomyocytes at individual dyads. Indeed, while linescan imaging of Ca^{2+} transients can provide insights into regional regulation of Ca^{2+} release, including by hormonal agonists, a heavy cytosolic buffering to restrict Ca^{2+} signal to the site of generation is required to shed light on the activity of individual dyads (Song et al., 1998). Although used for analysis of dyadic Ca^{2+} dynamics during ECC, the capacity for GCaMP6f–triadin to detect hormonally induced changes in Ca^{2+} release kinetics in the dyad has not, however, previously been tested.

Here, we demonstrated the utility of GCaMP6f–triadin to detect the changes in the expected dyadic Ca^{2+} fluxes induced by catecholamines and then took advantage of this property to assess the effect of stimulation with ET-1 and $InsP_3$ on dyadic Ca^{2+} signals in rat ventricular cardiomyocytes. Using live-cell imaging of dyadic Ca^{2+} transients, we showed that ET-1 increased spatial recruitment and Ca^{2+} flux at individual release sites, independently of SR Ca^{2+} load. Importantly, augmented dyadic Ca^{2+} release was attenuated by $InsP_3R$ inhibition. Furthermore, we demonstrated increased frequency of Ca^{2+} sparks in response to ET-1, using the dyadic reporter, indicating their localization to this domain. Together, our results suggest that IICR signals to RyRs in the dyad, thereby increasing the likelihood of their activation and SR Ca^{2+} release. We propose that, through this mechanism, ET-1 elicits its effects to increase the fidelity of release site activation and to augment dyadic SR Ca^{2+} release fluxes.

RESULTS

GCaMP6f–triadin reports Ca^{2+} changes at individual dyads during the Ca^{2+} transient

Appropriate targeting of GCaMP6f–triadin to the dyad in rat ventricular cardiomyocytes was first assessed by confocal imaging. Analysis of deconvolved confocal images revealed a striated distribution of GCaMP6f–triadin throughout the cardiomyocyte volume (Fig. 1i). Through examination of GCaMP6f–triadin distribution in cardiomyocytes immunostained with antibodies against the type 2 RyR (RyR2) and the sarcolemmal and TT proteins [NCX (herein referring to the cardic isoform NCX1, also known as SLC8A1) and Cav3], the reporter was found to be mainly associated with RyRs that colocate with TTs (junctional RyRs) (Fig. 1ii). There is a high degree of colocalization of GCaMP6f–triadin with RyRs as exhibited by the substantial overlap of the fluorescence signal of the two fluorescence channels observed in the images (Fig. 1ii) and quantified through Manders' colocalization analysis, which showed overlap of 90±1.2% (mean±s.e.m.) of GCaMP6f–triadin with RyRs and 73±4.4% of RyR with GCaMP6f. By distance analysis, 70% of GCaMP6f–triadin was found to be

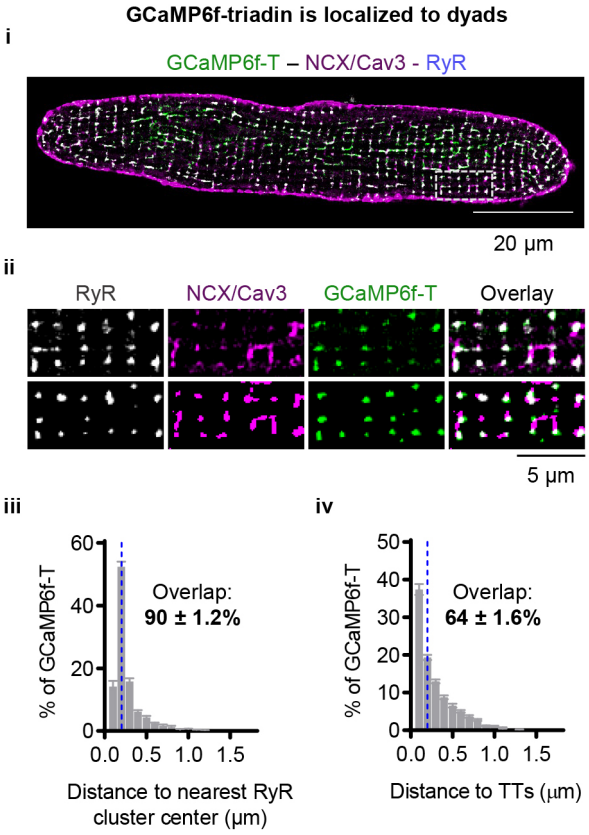

Fig. 1. GCaMP6f–triadin is localized to the dyad in cardiomyocytes. Analysis of GCaMP6f–triadin distribution in rat cardiomyocytes at 48 h post infection. (i) Mid-plane image of deconvolved confocal *Z*-stack of cardiomyocyte overexpressing GCaMP6f–triadin (GCaMP6f-T) (green) with TTs and sarcolemma delineated by NCX and Cav3 labeling in magenta, and RyR labeling in gray. (ii) Magnified view of the section demarcated by the white square in i. Top are deconvolved confocal images and bottom are masks of the deconvolved images showing the distribution of each protein alone and in overlay. (iii) Percentage of GCaMP6f–triadin puncta as a function of the Euclidean distance from the center of the nearest RyR cluster. (iv) Distribution of distances between centers of NCX/Cav3 and GCaMP6f–triadin puncta. Left of the dashed line are bars indicating distances between centroids that are considered to colocalize. Mean±s.e.m.; *n*=34 cells, *N*=5 animals.

Journal of Cell Science

Journal of Cell Science (2021) 135, jcs258671. doi:10.1242/jcs.258671

located within 0.2 µm of the nearest RyR cluster center (Fig. 1iii). In addition to proximity to RyRs, ∼56% of the GCaMP6f–triadin fluorescence was within 0.2 µm of the skeletonized TTs (Fig. 1iv) (cf. to 48% of RyR). In agreement with the distance-based analysis, Manders' colocalization analysis of the two labels showed a 64±1.6% overlap of GCaMP6f–triadin with TTs. Together, the overlap of the majority of GCaMP6f–triadin with TTs and RyRs is consistent with its appropriate targeting to dyadic junctions.

Fluorescence responses of GCaMP6f–triadin were next compared with those of non-targeted GCaMP6f, according to the experimental protocol outlined in Fig. 2A. Consistent with reporting of dyadic Ca^{2+} changes during ECC, GCaMP6f–triadin displayed rapid increases in fluorescence at punctate sites across the cell that tracked electrical pacing (Fig. 2Bi). In comparison with the fluorescence changes of non-targeted GCaMP6f during the Ca^{2+} transient, cell-averaged fluorescence changes of GCaMP6f–triadin exhibited a more rapid rate of rise and were 2-fold greater in amplitude (Fig. 2Ci,ii). Given that GCaMP6f–triadin Ca^{2+} affinity is not substantially affected by fusion to triadin (Shang et al., 2014), these data are consistent with greater proximity of GCaMP6f–triadin to dyadic release sites with higher Ca^{2+} concentration than the non-targeted GCaMP6f.

GCaMP6f–triadin fluorescence changes at individual dyads during Ca^{2+} release were next analyzed. The maximal first derivative of the fluorescence increase of the reporter during the upstroke of the Ca^{2+} transient was used as a measure of Ca^{2+} release flux (the maximal rate of Ca^{2+} release). Since this measure preceded substantial contraction, it was not affected by cardiomyocyte contraction and dyad movement. As a measure of synchronicity or temporal dispersion of Ca^{2+} release between dyads, the mean and standard deviation of the latencies of Ca^{2+} release between individual sites and the first Ca^{2+} release site detected in a cell were used. These analyses revealed a substantial temporal dispersion in release site activation and in maximal Ca^{2+} release flux between dyads (Fig. 2Bii; Fig. S2A,B). To further probe the advantage of the dyad targeting for measurements of Ca^{2+} responses, responses of non-targeted GCaMP6f at dyadic regions demarcated using the membrane stain Di-8-ANEPPS were also analyzed. While heterogeneity of release site activation was detected using GCaMP6f, it was substantially lower than for GCaMP6f–triadin (Fig. S2A). Ca^{2+} flux measured with GCaMP6f was also significantly lower and showed less variation between release sites than that measured using GCaMP6f–triadin (Fig. S2B).

To explore the potential for using GCaMP6f–triadin to detect changes in dyadic Ca^{2+} dynamics, its ability to detect alterations in dyadic Ca^{2+} flux during ECC in response to robust stimulation with β-adrenergic agonist (osoproterenol; Iso) was first investigated. Cell-averaged measurements of GCaMP6f–triadin showed increases in Ca^{2+} flux and Ca^{2+} amplitude of the Ca^{2+} transients following Iso stimulation (Fig. 2Ci,ii). Effects of Iso stimulation were also detected using the non-targeted GCaMP6f but were substantially smaller (Fig. 2Ci,ii). Ca^{2+} dynamics at individual dyads during Iso stimulation was next investigated. Using GCaMP6f–triadin, significant increases in the sensitivity of SR Ca^{2+} release onset, synchrony of release site activation, maximal dyadic Ca^{2+} release flux and the number of active sites were detected in response to Iso (Fig. 2Di–iv). The magnitude of the Iso effects were significantly smaller for the non-targeted GCaMP6f at Di-8-ANNEPS-labeled sites, and no inter-site heterogeneity in activation was detected (Fig. 2Di,ii).

Together, these data highlight the requirement for proximity of the reporter to the dyadic nanodomain to gain insights into Ca^{2+} release kinetics, free from contamination by indicator mobility, Ca^{2+} diffusion and cytosolic Ca^{2+} buffering. These data further indicate that GCaMP6f–triadin is a reliable tool to analyze the spatial and temporal synchrony of Ca^{2+} release between dyads and their modulation by hormonal agonists.

The activity and number of dyadic Ca^{2+} release sites during electrically evoked Ca^{2+} transients are increased by ET-1 independent of SR Ca^{2+} load

Whether alterations in dyadic Ca^{2+} dynamics contribute to the actions of ET-1 on ECC-associated Ca^{2+} transients was next determined according to the protocol indicated (Fig. 3A). Spatially averaged cell-wide measurements of dyad-targeted (Fig. 3B,Ci,ii) and non-targeted GCaMP6f (Fig. S3A) both reported significant increases in the rate of rise and amplitude of the whole-cell Ca^{2+} transient, consistent with previous findings using inorganic Ca^{2+} indicators (Harzheim et al., 2009; Proven et al., 2006). As previously described (Proven et al., 2006; Zima and Blatter, 2004), not all cells responded to ET-1 with an alteration in Ca^{2+} transient properties. Specifically, increases in Ca^{2+} transient amplitude and maximal Ca^{2+} release flux were detected in 11/17 and 15/18 cardiomyocytes using the dyad-targeted (Fig. 3Ci,ii) and non-targeted reporters (Fig. S3Aii,iii). In the absence of ET-1, no changes in kinetics or amplitude of the Ca^{2+} transient were detected with either the dyad-targeted or non-targeted reporter (Fig. S3A,B).

The enhanced dyadic Ca^{2+} release kinetics in the ET-1-responding cell population could result from enhanced synchronization of Ca^{2+} release between sites, increased recruitment of release sites and/or increased maximal Ca^{2+} release flux at individual sites. To test between these possibilities, we analyzed GCaMP6f–triadin responses at individual dyads before and after ET-1 stimulation. Analysis of the mean±s.d. of the latency of Ca^{2+} release revealed no significant effect of ET-1 on Ca^{2+} release site synchrony (Fig. 3Ciii,iv). As indicated by the greater number of lines of high GCaMP6f–triadin fluorescence intensity on the xt plot (kymograph) (Fig. 3Bi), ET-1 exposure for 10 min induced a significant increase in the number of active Ca^{2+} release sites (Fig. 3Cv). No changes in these parameters were observed in control cardiomyocytes perfused with buffer alone for 10 min (Fig. S3C).

Consistent with its enhancement of SR Ca^{2+} release, ET-1 application also increased maximal Ca^{2+} release flux at individual dyads (Fig. 3Di). After ET-1 application, the variability in maximal Ca^{2+} release flux between dyads was, however, significantly increased, as shown in the frequency distribution of maximal Ca^{2+} release flux at individual release sites (Fig. 3Dii). Whether the greater heterogeneity of maximum Ca^{2+} release flux following ET-1 application arose due to alteration in the properties of individual release sites or as a result of recruitment of more sites with heterogeneous properties was next investigated. To this end, the effect of ET-1 on the variability of Ca^{2+} release between sites (inter-site) during a Ca^{2+} transient and at individual release sites (intra-site) during consecutive beats was determined. Under control conditions, a substantial variation in maximal Ca^{2+} release flux at individual dyads and between successive beats was observed. Intra-site variability during consecutive Ca^{2+} transients was, however, greater than inter-site variability during a single Ca^{2+} transient (Fig. 3Fi–iii). While ET-1 stimulation did not affect the inter-site variability in the maximal Ca^{2+} release flux [illustrated by the coefficient of variance (CV)] between different Ca^{2+} release sites (Fig. 3Fii), it significantly reduced the variability in maximal

Journal of Cell Science (2021) 135, jcs258671. doi:10.1242/jcs.258671

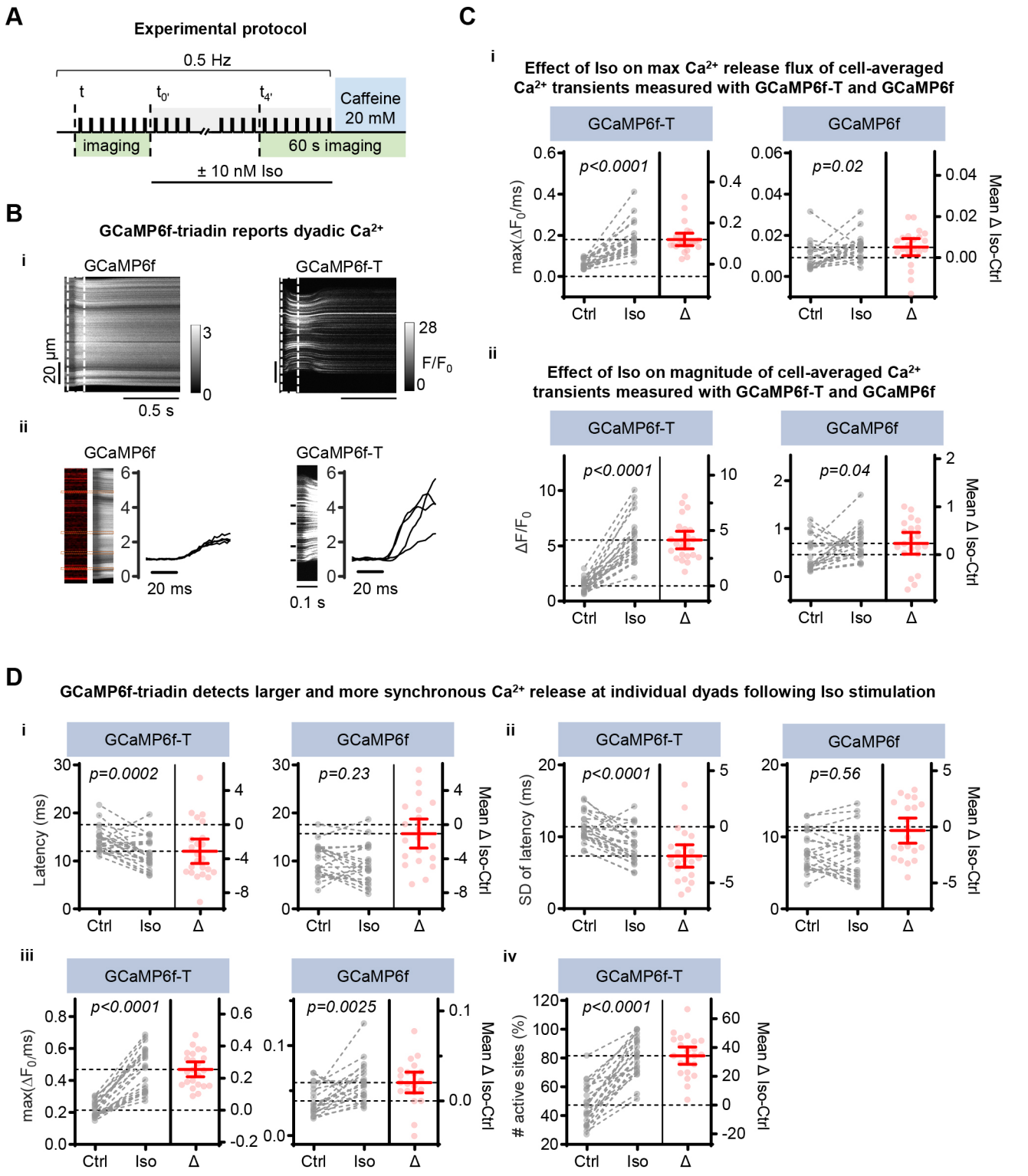

Fig. 2. See next page for legend.

Ca^{2+} release flux at individual dyads between Ca^{2+} transients (Fig. 3Fiii).

Whether an increase in SR Ca^{2+} load contributed to the augmentation of dyadic Ca^{2+} release by ET-1 was next tested. To this end, the effect of ET-1 on the maximal dyadic Ca^{2+} release flux induced by caffeine, which induces opening of all RyRs independently of sarcolemmal depolarization (Smith et al., 1988), was next examined. By exhausting the SR Ca^{2+} store, this approach informs on SR Ca^{2+} load and location of SR Ca^{2+} release sites, including those that are not directly coupled to sarcolemmal depolarization. Consistent with its expected mode of action, rapid local application of 20 mM caffeine increased the fluorescence intensity at all dyads demarcated by expression of the targeted Ca^{2+} biosensor, indicating activation of these release sites and release of

Journal of Cell Science (2021) 135, jcs258671. doi:10.1242/jcs.258671

Fig. 2. Dyad targeting of GCaMP6f is required to detect synchronization of Ca^{2+} release during ECC in ventricular cardiomyocytes following β-adrenergic stimulation. (A) Protocol used for assessment of kinetics and synchrony of dyadic Ca^{2+} release during ECC with and without Iso. (B) Assessment of dyadic Ca^{2+} signals with non-targeted GCaMP6f and GCaMP6f–triadin obtained by confocal linescan imaging. (i) Representative xt plots of fluorescence changes of non-targeted GCaMP6f (left) and GCaMP6–triadin (right) after treatment with Iso. (ii) Magnified view of the xt plot region depicted by dashed line in i. Right of the respective xt plots are the corresponding profiles of the fluorescence changes detected at junctional release sites from the indicated regions. For non-targeted GCaMP6f, fluorescence is plotted from TT regions labeled with di-8-ANEPPS. (C) Modulatory effect of Iso on Ca^{2+} release during ECC reported by GCaMP6f–triadin and non-targeted GCaMP6f. (i) Measurement of Ca^{2+} transient upstroke rate [max(ΔF_0/ms)] under Iso stimulation by GCaMP6f–triadin (left) and non-targeted GCaMP6f (right). (ii) Quantification of peak ($\Delta F/F_0$) of cell-wide averaged fluorescence changes recorded using GCaMP6f–triadin (left) and non-targeted GCaMP6f (right) before and after 4 min of Iso stimulation. (D) Ca^{2+} signals properties assessed by GCaMP6f–triadin (GCaMP6f-T) and non-targeted GCaMP6f following Iso stimulation. The latency (i) and synchrony (ii) of Ca^{2+} release, maximal Ca^{2+} release flux at single release sites (iii) and fraction of active dyads (iv) were determined. Data is presented as repeated measures before and after stimulation with the mean difference between the two groups and the 95% confidence interval of this mean. Each data point corresponds to the average value of a parameter from a single cell. Each measurement is the average of seven consecutive transients. Mean data are from $n_{cells}/N_{animals}$=23/5 for GCaMP6f–triadin and $n_{cells}/N_{animals}$=21/6 for non-targeted GCaMP6f. The number of release sites at baseline and after Iso application is 689/894 and 339/328 for GCaMP6f–triadin and non-targeted GCaMP6f, respectively. A paired *t*-test was used for statistical comparison of data.

available Ca^{2+} from the intracellular store (Fig. S3Di,ii). The maximal SR Ca^{2+} release flux following caffeine application was on average 2-fold greater than during electrical pacing (Fig. S3Diii). ET-1 stimulation did not significantly alter the peak of caffeine-induced Ca^{2+} release (Fig. 3E), consistent with an effect of ET-1 on dyadic Ca^{2+} independent of an increase in the SR releasable Ca^{2+}.

Together, these data highlight the plasticity of individual dyads and support the notion that ET-1 augments SR Ca^{2+} release via a mechanism involving recruitment of normally 'silent' release sites and by enhancing Ca^{2+} flux at them, suggesting that more RyRs and/or RyR clusters are activated synchronously among or within release sites.

$InsP_3R$ activation underlies increased recruitment of Ca^{2+} release sites by ET-1

The contribution of $InsP_3Rs$ to the enhancement of dyadic Ca^{2+} release by ET-1 was next determined. Our previous studies show the presence of populations of $InsP_3Rs$ that are proximal to RyRs (Harzheim et al., 2009), but their location relative to the dyad and RyRs within the dyad was not determined. Confocal imaging of $InsP_3Rs$ and RyRs in cardiomyocytes immunolabeled with antibodies that recognize the type 2 isoforms of these receptors revealed an overlap of 49.9±1.6% (mean±s.e.m.) of the two channel types as well as a proportion of $InsP_3Rs$ located between RyR clusters, albeit along the same Z-line (Fig. 4Ai). Consistent with this observation, similar findings regarding the relative distributions of these channels were obtained using a distance-based analysis (Fig. 4Aii). The location of $InsP_3Rs$ relative to TTs, was next analyzed by confocal imaging of $InsP_3Rs$ labeled using the same anti-type 2 $InsP_3R$ antibody used in Fig. 4Ai and TTs immunolabeled using an NCX and Cav3 antibody cocktail. By this analysis, 32±0.7% of $InsP_3Rs$ were found to overlap with TTs (Fig. 4Aiii). In line with these data, distance-based analysis of $InsP_3R$ and TT localization revealed ∼30% of $InsP_3Rs$ to be located <0.2 µm from TTs (Fig. 4Aiv). This observation suggests that, because of close localization, Ca^{2+} signals through $InsP_3R$ could influence Ca^{2+} release via RyRs clusters. In line with the overlap of $InsP_3Rs$ and RyRs with the TTs, immunofluorescent labeling revealed significant colocalization of GCaMP6f–triadin with the $InsP_3R2$ (Fig. 4Ai,ii).

The influence of $InsP_3Rs$ on dyadic Ca^{2+} was examined. To this end, IICR was either stimulated by ET-1 application or suppressed by co-application of the $InsP_3R$ inhibitor 2-aminoethoxydiphenyl borate (2-APB) according to the protocol indicated (Fig. 4B). 2-APB was used at a relatively low concentration of 2 µM previously shown to inhibit $InsP_3Rs$ without effects on pacing-induced Ca^{2+} transients in cardiomyocytes (Peppiatt et al., 2003). Consistent with the hypothesis that dyadic Ca^{2+} dynamics were influenced by ET-1-stimulated IICR, 2-APB abrogated the increased maximal Ca^{2+} release flux integrated across all dyadic sites during the Ca^{2+} transient elicited by its application (Fig. 4C,Di). In control experiments, no effects of 2-APB on these parameters were detected (Fig. S4A,B).

The consequence of $InsP_3R$ inhibition on maximal Ca^{2+} release flux and its heterogeneity at individual Ca^{2+} release sites in cardiomyocytes exposed to ET-1 was next assessed. To allow direct comparison between conditions, measurements at 10 min after treatment were normalized to those before. ET-1 application increased the maximal Ca^{2+} release flux at individual dyads, which was inhibited by 2-APB (Fig. 4Dii). 2-APB application also reduced the number of active release sites during ECC in ET-1-stimulated cells (Fig. 4Diii). Application of 2-APB alone did not affect dyadic maximal Ca^{2+} release flux (Fig. S4C–F). Similarly, 2-APB application did not show any effect on SR releasable Ca^{2+}, as determined by caffeine-induced SR Ca^{2+} release (Fig. 4Div). Together, these data indicate that Ca^{2+} release via $InsP_3Rs$ in the vicinity of dyadic RyRs mediates the increase in maximal Ca^{2+} flux and sensitivity of local dyadic SR Ca^{2+} release as well as the spatial recruitment of active release sites observed in ET-1-stimulated cardiomyocytes.

ET-1 stimulation induced more frequent and larger Ca^{2+} sparks in quiescent ventricular cardiomyocytes

To further examine $InsP_3R$–RyR interactions in dyadic Ca^{2+} release, elementary Ca^{2+} release events were analyzed. As Ca^{2+} sparks are the building blocks of the Ca^{2+} transient generated via the coordinated activation of RyRs, their analysis provides information regarding how activation of $InsP_3Rs$ influences the overall Ca^{2+} release process. In these experiments, as the Ca^{2+} reporter is dyadic, Ca^{2+} release events are highly localized with dyadic RyR clusters, and have been termed nanosparks (Shang et al., 2014).

Ca^{2+} nanosparks were recorded in quiescent intact ventricular cardiomyocytes, following 10 min pacing, in the presence of buffer or ET-1 (according to the protocol in Fig. 5Ai). Representative recordings of Ca^{2+} nanosparks are shown in the xt plot images and F/F_0 traces in Fig. 5Aii,iii. As shown in the xt plot images, Ca^{2+} nanosparks were reported at dyadic sites of GCaMP6f–triadin localization. As would be expected following conditioning with low pacing frequency, Ca^{2+} nanosparks were relatively rare under control conditions (observed in 11/16 cardiomyocytes) (Fig. 5Aii, Bi). The frequency of these events was, however, significantly increased following ET-1 application (15/16 cardiomyocytes displayed Ca^{2+} release events) (Fig. 5Aiii,Bi). The spatiotemporal properties of the Ca^{2+} nanosparks were not affected by ET-1, while their associated maximal Ca^{2+} release flux was significantly larger (Fig. 5Bii,vi). Although, the means of the amplitudes and full width at half maximum (FWHM) of Ca^{2+} nanosparks were unaffected by

Journal of Cell Science (2021) 135, jcs258671. doi:10.1242/jcs.258671

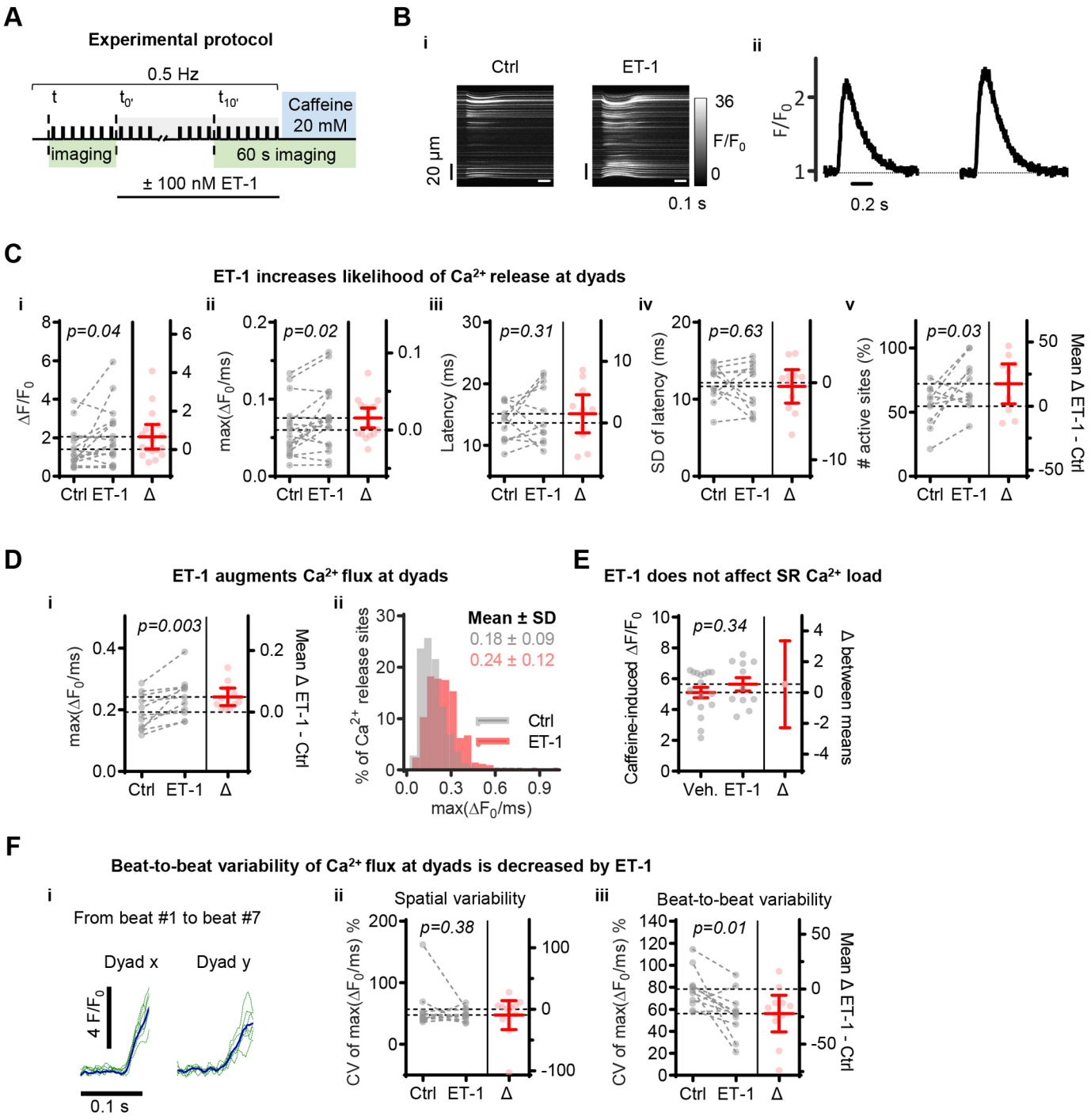

Fig. 3. ET-1 stimulation increases Ca^{2+} release sites recruitment and their rate of Ca^{2+} release in electrically paced ventricular cardiomyocytes. (A) Protocol used for evaluation of ET-1 effects on dyadic SR Ca^{2+} release during ECC. (B) Confocal linescan imaging of changes in GCaMP6f–triadin fluorescence before and after 10 min of ET-1. Representative xt plots (i) and corresponding normalized fluorescence traces (ii) are presented. (C) Quantification of spatiotemporal synchronicity of release site activation. (i) Peak and (ii) maximal Ca^{2+} release [max(ΔF_0/ms)] of cell-wide Ca^{2+} transients; (iii) latency of Ca^{2+} release onset; (iv) mean deviation of latency of Ca^{2+} release; (v) the percentage of active release sites normalized to the maximal number of potential release sites determined by caffeine application. (D) Effects of ET-1 on SR Ca^{2+} release kinetics. (i) Mean max(ΔF_0/ms) flux with and without ET-1. (ii) Distribution of max(ΔF_0/ms) at single release sites before and after stimulation with ET-1. (E) Peak caffeine-induced Ca^{2+} release with and without ET-1 treatment. (F) Max(ΔF_0/ms) variance between dyads and at the same dyad between consecutive beats. (i) Superimposition of seven consecutive Ca^{2+} transients recorded from three different scanned release sites at baseline. The thick blue line indicates the average fluorescence change at a single release site. (ii) Quantification of the spatial variability of max(ΔF_0/ms) between single release sites before and after application of ET-1. (iii) Quantification of max(ΔF_0/ms) variability between beats at individual dyad before and after ET-1. The effect of treatment was examined by paired *t*-test. SR Ca^{2+} content was compared by an unpaired *t*-test. The differences in distributions of max(ΔF_0/ms) at individual release sites was determined with an equal variance (F) test. Except for the panels Ci,ii (data from $n_{cells}/N_{animals}$=17/4), mean data are from $n_{cells}/N_{animals}$=11/4 and $n_{cells}/N_{animals}$=18/5 for the ET-1-treated and control groups, respectively. *n* of release sites at baseline and 10 min post-stimulation with ET-1 is 624/669.

Journal of Cell Science (2021) 135, jcs258671. doi:10.1242/jcs.258671

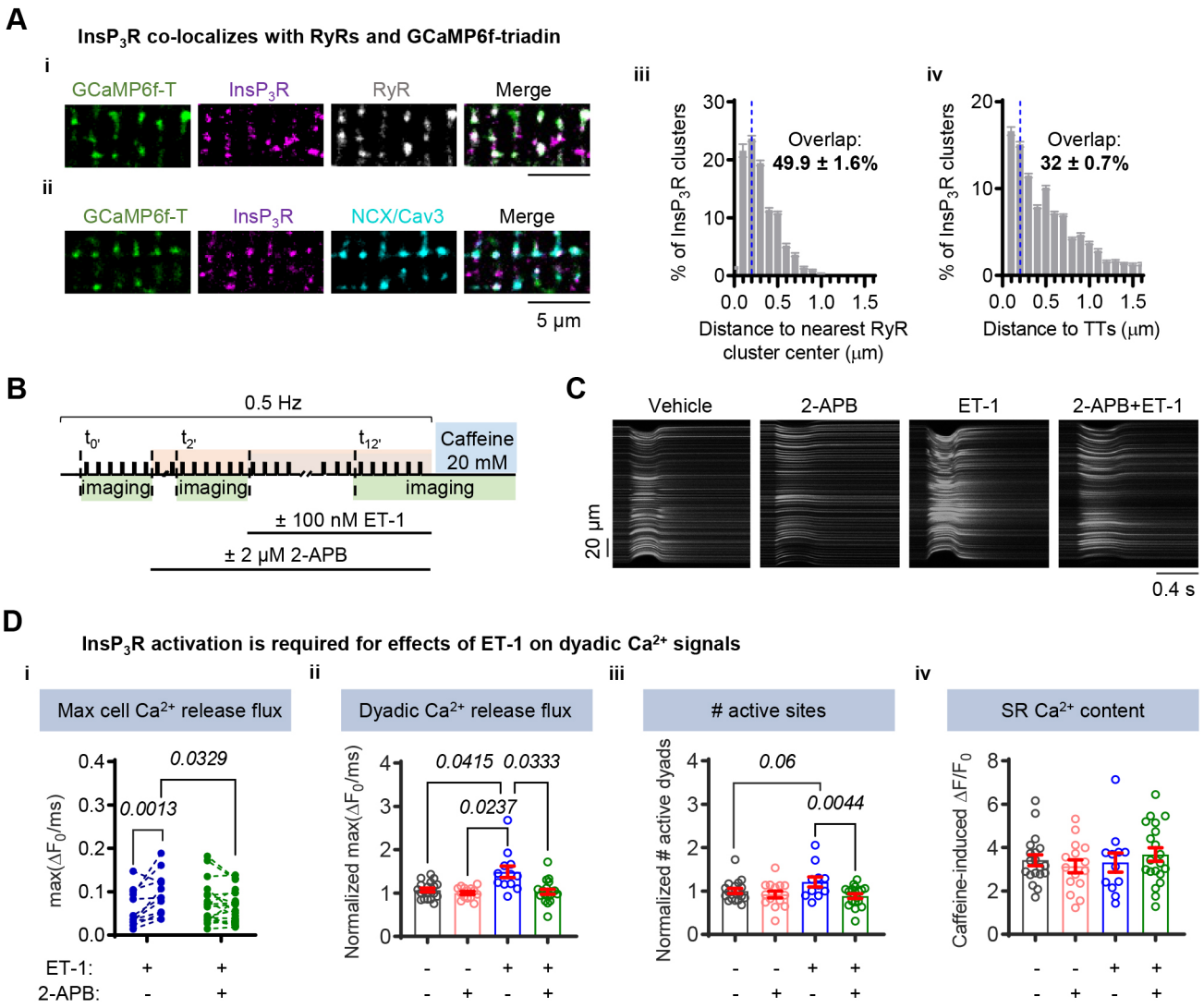

Fig. 4. Ca^{2+} release via $InsP_3Rs$ is required for the modulation of dyadic Ca^{2+} signals by ET-1. (A) Confocal immunofluorescence analysis of $InsP_3R$ distribution relative to RyRs, TTs (visualized by co-staining for NCX1 and Cav3) and GCaMP6f–triadin in cardiomyocytes. (i) View showing relationship between GCaMP6f–triadin (green), $InsP_3Rs$ clusters (magenta) and RyRs clusters (gray). (ii) View showing the spatial relationship between GCaMP6f–triadin (green), $InsP_3Rs$ clusters (magenta) and TTs (cyan). (iii) Histogram of distances between $InsP_3R$ and their nearest RyRs clusters. The dashed line indicates the threshold distance between cluster centers below which clusters are considered to colocalize. Data are from n_{cells}=21 and $N_{animals}$=3. (iv) Histogram of distances between $InsP_3R$ and nearest TTs. Data are from n_{cells}=22 and $N_{animals}$=3. Mean±s.e.m. (B) Protocol for probing the contribution of IICR to the modulation of dyadic SR Ca^{2+} by ET-1. (C) Confocal linescan imaging of GCaMP6f–triadin fluorescence showing Ca^{2+} transients under the different conditions are shown. (D) Analysis of effects of ET-1±2-APB on dyadic Ca^{2+} dynamics. (i) Max(ΔF_0/ms) of the Ca^{2+} transient. (ii–iv) The relative change in (ii) dyadic max(ΔF_0/ms), (iii) percentage of active release sites normalized to baseline and (iv) magnitude of caffeine-induced SR Ca^{2+} release are shown. Data are given as repeated measures with each dot representing a single cell in panel Di and as mean±s.e.m. in Dii–iv. Groups were compared by two-way repeated measures ANOVA with Bonferroni post hoc testing (Di), one-way ANOVA test (Dii–iv). Data are from n_{cells}=16, 14, 12 and 18; $N_{animals}$=4 for control, 2-APB, ET-1 and ET-1+2-APB, respectively.

ET-1, a significant increase in the variance of these measures was observed (P=0.0001 and P<0.0001 for amplitude and FWHM, respectively). The distribution of FWHM was also broader than in control, revealing a subpopulation of smaller Ca^{2+} release events (Fig. 5Biii). Interestingly, a population of Ca^{2+} nanosparks with FWHM ranging between 0.99 and 1.6 µm (those typically observed under control conditions) were of larger amplitude in ET-1-treated cells (Fig. 5C), suggesting an increased recruitment of RyRs. To uncover whether the limited changes in Ca^{2+} nanospark parameters observed in ET-1-stimulated cells impacted dyadic Ca^{2+} signaling, their signal mass ($1.206\times\Delta F/F_0\times FWHM^3$) (Chandler et al., 2003), which reflects the quantum of Ca^{2+} released with each event, and spark-mediated Ca^{2+} leak (product of mass and frequency) were calculated. ET-1 treatment did not, however, significantly alter Ca^{2+} nanospark mass or associated leak (Fig. 5D).

The requirement for RyRs for the action of ET-1 was next investigated. Tetracaine inhibition of RyRs resulted in an almost complete inhibition of Ca^{2+} nanosparks in control cells as well as in cells exposed to ET-1 (Fig. 5Bi). In the few remaining Ca^{2+} release events detected under control and ET-1-stimulated conditions, RyR inhibition also resulted in significant decreases in the amplitude, size (FWHM), duration (full duration half maximum; FDHM) and rise time (TTP). Maximal Ca^{2+} release flux of these events was not affected however (Fig. 5Bii–vi). As the analysis of Ca^{2+} release event properties in RyR inhibited cells is based on very few events in a few cells, effects of ET-1 cannot be ruled out.

Journal of Cell Science (2021) 135, jcs258671. doi:10.1242/jcs.258671

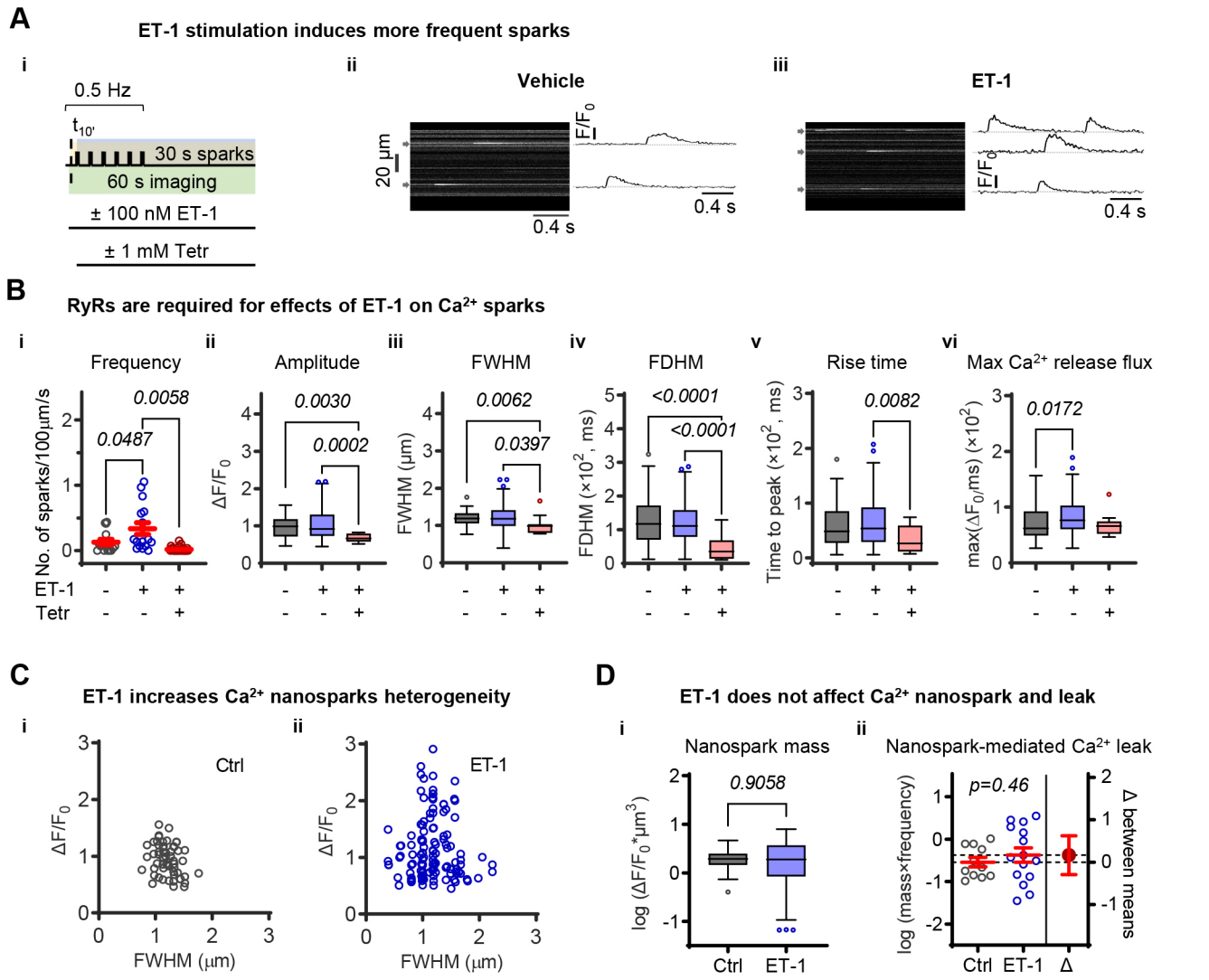

Fig. 5. ET-1 stimulation induces more frequent and heterogeneous Ca^{2+} nanosparks in quiescent rat ventricular cardiomyocytes. (A) Measurement of Ca^{2+} nanosparks with GCaMP6f–triadin. (i) Experimental protocol used for analysis of Ca^{2+} nanosparks upon stimulation with ET-1. (ii) Confocal linescan imaging under control conditions and (iii) after treatment with 100 nM ET-1. Local changes in (F/F_0) from the release sites indicated by the gray lines are on the right of the xt plots. (B) Effects of ET-1 with and without tetracaine (Tetr) on Ca^{2+} nanospark frequency and spatiotemporal properties of Ca^{2+} nanosparks. (i) Frequency of Ca^{2+} nanosparks, (ii) amplitude, (iii) size, (iv) duration, (v) rise time and (vi) maximal Ca^{2+} release flux. (C) Scatter plot of Ca^{2+} nanospark amplitude in relation to size under control (i) and following ET-1 treatment (ii). (D) Quantification of Ca^{2+} nanospark mass (i) and Ca^{2+} leak (ii) under control and treatment with ET-1. Data in Bi and Dii is presented as mean±s.e.m., in Bii–vi and Di as Tukey boxplots with median values under control conditions and following stimulation with ET-1 with or without tetracaine. Groups in Bi were compared with Brown–Forsythe and Welch ANOVA test. Differences in the Ca^{2+} nanospark properties (panels Bii–vi) were compared with Kruskal–Wallis test. Difference between means in Di and Dii were assessed with Mann–Whitney and unpaired *t*-test, respectively. Data are from n_{cells}=16, 16 and 31, $N_{animals}$=6, n_{events}=54 (11 cells), 142 (15 cells) and 16 (9 cells) for control, ET-1 and ET-1+tetracaine-treated group, respectively.

Together, these data support the notion that ET-1 augments dyadic Ca^{2+} nanospark frequency via stimulation of Ca^{2+} release through $InsP_3Rs$ and its activation of RyRs.

Direct $InsP_3R$ activation evoked more frequent and heterogeneous Ca^{2+} nanosparks

To probe the functional interaction between $InsP_3Rs$ and RyR and its regulation of dyadic Ca^{2+} signaling independent of other cellular consequences of ET-1 stimulation, Ca^{2+} release via $InsP_3Rs$ was directly induced by $InsP_3$ liberated from a caged precursor (cag-$InsP_3$) (Fig. 6A). Uncaging of $InsP_3$ resulted in an increase in Ca^{2+} nanospark frequency in individual cells when compared to controls (Fig. 6Bi). No effect of $InsP_3$ uncaging on the amplitude, duration (FDHM), rise time (time to peak, TTP) and maximal Ca^{2+} release flux of nanosparks was detected, while their size (FWHM) was decreased (Fig. 6Bii–vi). $InsP_3$ uncaging did, however, induce an increase in the variance in amplitude (P=0.0106) and FWHM (P<0.0001) of the Ca^{2+} nanosparks (Fig. 6Bii,iii). No effect of $InsP_3$ uncaging on Ca^{2+} nanospark mass and Ca^{2+} leak was detected (Fig. 6Bvii,viii). The above results suggest that IICR increases the probability of Ca^{2+} nanospark generation at dyadic sites by both recruiting RyR clusters and more RyRs within a cluster.

The effects of direct stimulation of $InsP_3Rs$ on dyadic Ca^{2+} in the absence of RyRs activation were next examined. To this end, Ca^{2+} release events were recorded with RyR inhibition according to the protocol outlined in Fig. 6C. Application of tetracaine alone led to an almost complete cessation of Ca^{2+} release events. The few remaining events had a lower FWHM than those detected in control

Journal of Cell Science (2021) 135, jcs258671. doi:10.1242/jcs.258671

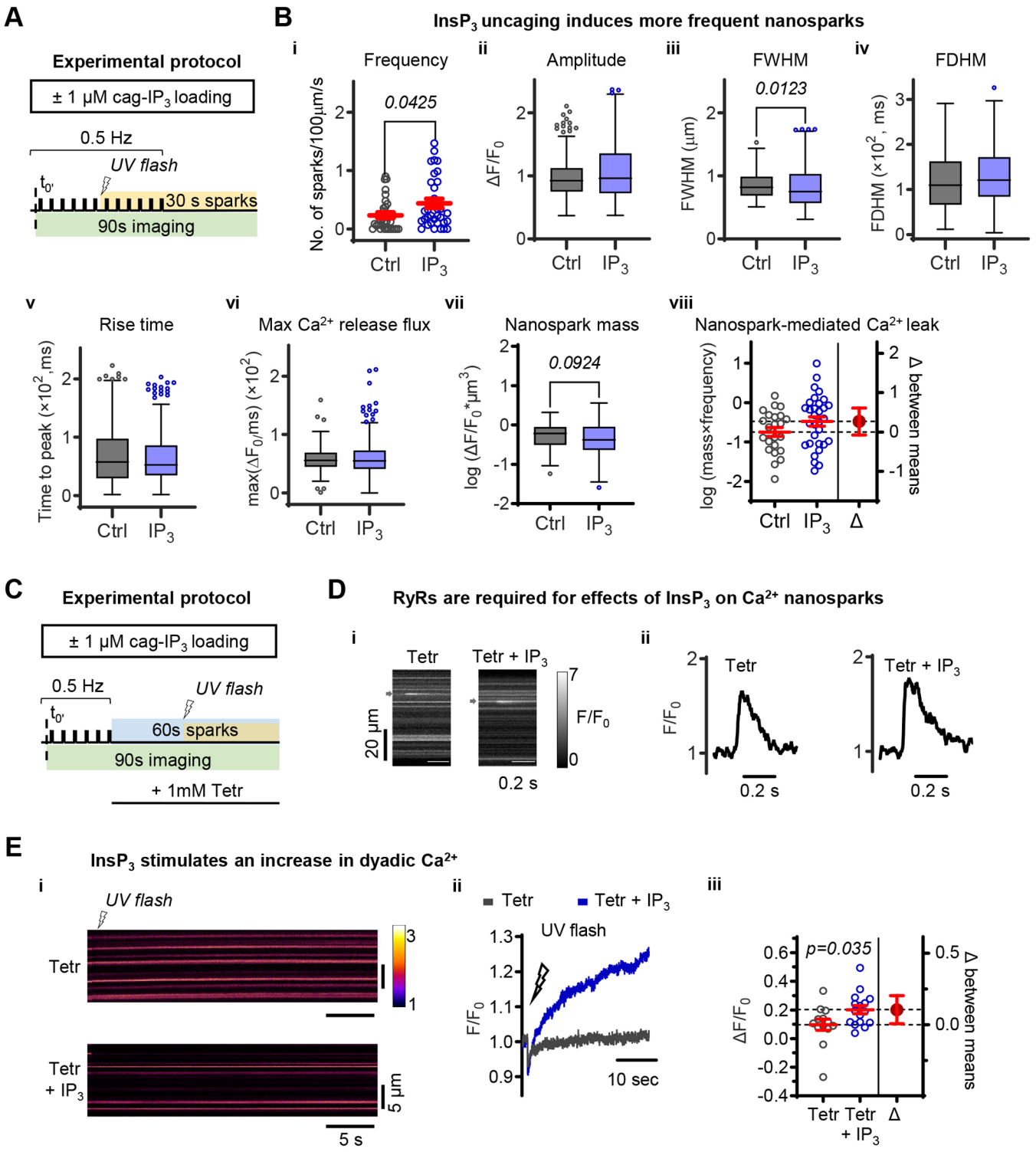

Fig. 6. Photo-release of $InsP_3$ evokes more frequent dyadic Ca^{2+} release events/nanosparks. (A) Protocol used to assess frequency and properties of dyadic Ca^{2+} release events following photo-release of $InsP_3$. (B) Frequency and properties of Ca^{2+} release events following photo-release of $InsP_3$. (i) Average data of the effects of $InsP_3$ on Ca^{2+} release event incidence and (ii–vii) Tukey boxplots with median values for amplitude (ii), FWHM (iii), FDHM (iv), time to peak (v), maximal Ca^{2+} release flux (vi) and mass (vii) of Ca^{2+} release events. (viii) Average data of nanospark-mediated Ca^{2+} leak. Data are from n_{cells}=32 and 33, $N_{animals}$=4, n_{events}=156 (23 cells) and 323 (31 cells) for control and $InsP_3$-treated group, respectively. (C) Protocol used for the analysis of dyadic SR Ca^{2+} following $InsP_3$ uncaging with or without RyR blockade with tetracaine (Tetr). (D) Confocal linescan imaging of GCaMP6f-triadin fluorescence. Representative xt plots (i) and fluorescence traces (ii) of rare Ca^{2+} release events after RyR inhibition. (E) In the presence of tetracaine, $InsP_3$ uncaging induces an increase in GCaMP6f–triadin fluorescence. (i) Representative xt plots of GCaMP6f–triadin fluorescence in cardiomyocytes loaded with or without caged $InsP_3$ after photo-stimulation. (ii) F/F_0 traces show a gradual increase in fluorescence after $InsP_3$ uncaging in the presence of tetracaine. Values are normalized to the first 100 ms after the 405 nm flash. (iii) The change in fluorescence ($\Delta F/F_0$) between a 1 s average of the signal immediately after uncaging and at the end of 30 s imaging period is shown. Cells with Ca^{2+} release events during this period were excluded from the analysis (4 and 3 cells for control and cells loaded with cag-$InsP_3$). Data is presented as mean ±s.e.m. n_{cells}=13 and 16, $N_{animals}$=4. Unpaired *t*-test.

Journal of Cell Science

Journal of Cell Science (2021) 135, jcs258671. doi:10.1242/jcs.258671

Table 1. Comparison of Ca^{2+} release events or nanosparks induced by $InsP_3$ in the presence of tetracaine

	Frequency of Ca^{2+} release events (sparks×100 μm^{-1}×s^{-1})	$\Delta F/F_0$	FWHM, μm	FDHM, ms	TTP, ms	max(ΔF_0/ms)	n_{events}/n_{cells} (Total # of examined cells)
Tetracaine	0.15±0.04	0.94±0.27	0.63±0.08	165±148	145±162	49±15	7/4 (13)
Tetracaine+IP_3	0.52±0.78	0.98±0.35	0.99±0.32**	139±50	102±76	74±28*	22/3 (17)

Data are presented as mean±s.d. Spatiotemporal characteristics analyzed include amplitude ($\Delta F/F_0$), FWHM, FDHM, and TTP and maximal Ca^{2+} release flux [max(ΔF_0/ms)]. *P<0.05, **P<0.01 (unpaired Student's t-test).

cells (Fig. 6D; Table 1). Owing to the low number of observed events and their great variability, we could not reliably conclude whether these Ca^{2+} release events arose from incompletely inhibited RyRs or through the opening of $InsP_3R$ clusters (Table 1). However, $InsP_3$ uncaging under conditions of RyR inhibition with tetracaine produced a gradual but significant increase in the fluorescence of the dyadic reporter that was not detected in control cardiomyocytes in which $InsP_3$ was not uncaged (Fig. 6E). This increase in fluorescence is shown as a small increase in fluorescence at dyadic sites (brighter regions) in the xt plots of raw fluorescence, and more clearly, in the profiles of fluorescence intensity normalized to pre photo-stimulation levels and the histograms of averaged data.

DISCUSSION

Here, we tested the hypothesis that signaling crosstalk between dyadic $InsP_3Rs$ and RyRs contributed to the actions of ET-1 on Ca^{2+} transients during ECC in ventricular cardiomyocytes. Our investigation was enabled through the use of a dyad-targeted GFP-based Ca^{2+} indicator, which allowed analysis of dyadic Ca^{2+} with high temporal and spatial resolution. The data generated provides, for the first time, an analysis of modulation of dyadic Ca^{2+} by neurohormonal agents and their signaling via $InsP_3Rs$ in intact cardiomyocytes. Applying this approach, we showed that ET-1 treatment recruits Ca^{2+} release sites and augments maximal Ca^{2+} release flux during ECC without modulating SR Ca^{2+} load. Furthermore, we demonstrated that activation of dyadic $InsP_3Rs$ is necessary for the action of ET-1 on kinetics of local Ca^{2+} signals. Moreover, we show that Ca^{2+} release via RyRs is required for the effect of IICR to be manifest.

Application of GCaMP6f–triadin to study dyadic Ca^{2+} signals

While electrophysiological and modeling approaches have provided quantitative insights into dyadic Ca^{2+} changes on a cell-wide level, analysis of Ca^{2+} release during ECC, particularly at individual dyads has been challenging (Acsai et al., 2011; Cannell et al., 2013). Contributing to the inaccessibility of dyadic Ca^{2+} dynamics to analysis by inorganic Ca^{2+} indicator dyes is dye diffusion and rapid dissipation of dyadic Ca^{2+} changes (Sipido and Wier, 1991; Song et al., 1998). To deal with these issues, Ca^{2+} changes have been measured at individual dyads through the use of a high-affinity Ca^{2+} dye in the presence of strong but slow buffer to restrict Ca^{2+} diffusion in the cytosol (Song et al., 1998). This technique is, however, disruptive to ECC and requires low frequency electrical stimulation (~0.1 Hz) to allow SR Ca^{2+} loading and buffer equilibration. Fundamental aspects of Ca^{2+} release can also be uncovered through analysis of Ca^{2+} sparks, although this is generally performed in the absence of electrical pacing. Genetically engineered Ca^{2+} probes targeted to the dyadic cleft (Despa et al., 2014; Shang et al., 2014) have enabled measurements of Ca^{2+} dynamics at individual dyads in intact cardiomyocytes under physiological conditions and have thus provided new insights into their activity during ECC. As we show here, dyad movement during cardiomyocyte contraction makes tracking of individual dyads for the full duration of a Ca^{2+} transient difficult, precluding accurate measurement of transient amplitude. The onset of Ca^{2+} release and maximal Ca^{2+} release flux, which provide important information regarding the sensitivity and magnitude of Ca^{2+} flux central to our study, occurred prior to the onset of substantial contraction, and could thus be used without interference. This allowed us to avoid using pharmacological inhibitors of contraction and their associated issues (Gwathmey et al., 1991; Kolega, 2004). Analysis of these parameters showed significant variability in the activation time of Ca^{2+} release and maximal Ca^{2+} release flux at individual dyads during ECC. These data likely reflect the reported differences in RyR density and distribution per cluster, the number of clusters per dyad and location relative to the TT membrane (Dries et al., 2013; Galice et al., 2018; Kolstad et al., 2018). The rapid equalization of Ca^{2+} across the contiguous SR store makes it unlikely that the heterogeneity of SR Ca^{2+} release is due to inhomogeneous SR Ca^{2+} loading (Picht et al., 2011). Consistent with this notion, heterogeneity of Ca^{2+} release between dyads was significantly reduced when caffeine was used to activate RyRs.

Using GCaMP6f–triadin, we report the first description of an enhancement and spatial synchronization of SR Ca^{2+} release specifically in the dyad during ECC in response to stimulation with the β-agonist isoproterenol. While recruitment and augmentation of dyadic Ca^{2+} release has been previously reported using inorganic dyes, these analyses were not based on measurements at individual dyads during ECC. Rather, these data came from regional analysis of Ca^{2+} release or were from Ca^{2+} spikes at low pacing frequency. Our new data and analysis therefore directly demonstrate the potential for using this reporter for analysis of changes in dyadic SR Ca^{2+} release in response to hormonal or pharmacological interventions. Thus, although the Ca^{2+}-binding properties of the reporter were considered not ideal for detection of the large and rapid changes in Ca^{2+} at the dyad, the detection of increase in spatiotemporal synchrony of SR Ca^{2+} release, augmented maximal Ca^{2+} release flux and recruitment of previously inactive dyads by β-agonists would, however, indicate the capacity of the reporter to sense these changes. Furthermore, increases in SR Ca^{2+} flux and number of active release sites were also detected after caffeine application, which rapidly and synchronously activates SR Ca^{2+} release, thus reducing variability due to desynchronized activation by Ca^{2+} entry across the sarcolemma. Considering the relatively high dissociation constant of GCaMP6f–triadin (K_d=632 nM), although lower than of synthetic dyes, and that Ca^{2+} reaches 10–100 μM in the dyad during CICR (Acsai et al., 2011; Shannon et al., 2004), rapid saturation of the reporter was expected. The relatively slow 'turn-on' kinetics (k_{on}~20 ms) of GCaMP6f (Chen et al., 2013; Helassa et al., 2016), which likely does not allow equilibration to the steady state at saturating but short transient Ca^{2+} increases, is suggested to allow it to report the Ca^{2+} changes occurring in the dyad.

Dyadic localization of the indicator was also sufficient to detect β-adrenergic-mediated enhancement of Ca^{2+} release during ECC

Journal of Cell Science (2021) 135, jcs258671. doi:10.1242/jcs.258671

in cell-wide analysis of linescan imaging experiments. Despite measurement of fluorescence changes at TT demarcated with a membrane dye, effects of β-adrenergic agonist were less apparent when a non-targeted GCaMP6f was employed. Specifically, in contrast to the more heterogeneous rise in local Ca^{2+} release at junctions between the TT and SR reported by the dyad-targeted GCaMP6f, Ca^{2+} signals among dyads across the cell (highlighted by membrane stain) were homogenous when measured by the non-targeted reporter. This difference is, however, likely to be explained by Ca^{2+} diffusion and the homogenous distribution of the non-targeted reporter. In particular, after release, Ca^{2+} rapidly diffuses from its source where it is detected by the homogenously distributed reporter. As our measure of latency represents the time difference between the release site studied and the first Ca^{2+} release detected, the lower latencies of the non-targeted reporter reflect the homogenization of detection of Ca^{2+} release when using such a reporter. Together, these data highlight the substantial advantages of using a dyad-targeted reporter to measure the influence of hormonal mediators on SR Ca^{2+} release and moreover to dissect out mechanisms of regulation of individual Ca^{2+} release sites in this process.

$InsP_3$-induced Ca^{2+} release raises dyadic Ca^{2+} facilitating RyR activation

Although IICR modulates Ca^{2+} transients during ECC following GPCR engagement, the mechanism by which the relatively small Ca^{2+} flux via $InsP_3Rs$ influences the bulk changes in Ca^{2+} mediated by RyRs during ECC is not fully determined. Indeed, the low conductance of $InsP_3Rs$ (~3-fold lower than RyRs) (Foskett et al., 2007; Zima and Blatter, 2004), together with a substantially lower expression level than RyRs would suggest little capacity to impact global Ca^{2+}. Consistent with this, $InsP_3R$ activation in cells in which RyRs are inhibited leads to the generation of either a low frequency of Ca^{2+} puffs or 'silent' events (Harzheim et al., 2009; Horn et al., 2013; Wullschleger et al., 2017; Zima and Blatter, 2004).

Remarkably, by using the dyadic targeted GCaMP6f to analyze Ca^{2+} release at individual dyads during the Ca^{2+} transient, we uncovered that ET-1 acted to both recruit more dyads and to augment Ca^{2+} flux at individual dyads during the Ca^{2+} transient. ET-1 did not influence dyadic Ca^{2+} dynamics in every cardiomyocyte, however, and the magnitude of change varied substantially among the cells. This high degree of variability was previously suggested to result from variation between cardiomyocytes in the expression and/or ratio of ET_A and ET_B receptors (Domeier et al., 2008; Proven et al., 2006; Zima and Blatter, 2004). In addition to enhanced spatial recruitment of dyads during the Ca^{2+} transient, ET-1 also reduced the variability in dyadic Ca^{2+} release between Ca^{2+} transients. These observations could be explained by increased cooperativity of RyRs or RyR clusters activity within the single release site and/or increased Ca^{2+} sensitivity of RyRs (Galice et al., 2018).

The capacity for ET-1 to influence dyadic Ca^{2+} was dependent on Ca^{2+} release via $InsP_3Rs$. The localization of $InsP_3Rs$ to dyadic sites, as reported here and previously, supports this activity of $InsP_3Rs$. As shown previously for effects on global Ca^{2+} transients and Ca^{2+} sparks, the augmentation of dyadic Ca^{2+} signaling by IICR downstream of ET-1 was sensitive to $InsP_3R$ inhibition with 2-APB. Furthermore, photoliberation of $InsP_3$ from a caged precursor was sufficient to modulate dyadic Ca^{2+}, ruling out the requirement for other downstream effectors of GPCR signaling. Using this approach, the frequency but no other properties, of dyadic Ca^{2+} release events was increased, suggesting enhanced recruitment of the machinery underlying Ca^{2+} sparks. In support of this notion, inhibition of RyRs prevented the action of $InsP_3$. These data are in agreement with conclusions drawn in previous studies that did not directly measure dyadic Ca^{2+} release. The data presented here, however, now demonstrate the important contribution of dyadic $InsP_3R$–RyR channel crosstalk to the mechanism by which $InsP_3Rs$ can influence global Ca^{2+} changes in healthy ventricular cardiomyocytes but that have little effect when acting alone. Several studies, including from our laboratory, have, however, detected Ca^{2+} release events (Ca^{2+} puffs) in the presence of RyR inhibition in atrial cardiomyocytes and ventricular cardiomyocytes of different animal species (Harzheim et al., 2009; Wullschleger et al., 2017; Zima and Blatter, 2004). $InsP_3R$ expression is, however, greater in the atrial and diseased ventricular cardiomyocytes in which these observations were made. In the present study, we were unable to directly resolve Ca^{2+} puffs. The amplitude of Ca^{2+} puffs is ~20% of Ca^{2+} sparks (Zima and Blatter, 2004), which approaches the signal-to-noise detection threshold of a confocal microscope. Although, Ca^{2+} puffs may be generated at clusters containing as few as two $InsP_3Rs$ in mammalian cells, a substantial increase in Ca^{2+} flux and frequency is observed when the number of $InsP_3Rs$ forming a cluster is greater (Dickinson et al., 2012). Considering the low abundance of functionally active $InsP_3R$ in healthy ventricular cardiomyocytes, it is therefore not surprising that Ca^{2+} puffs were only rarely detected in the absence of active RyRs. Instead, and consistent with induction of Ca^{2+} release via $InsP_3Rs$, we observed an increase in baseline Ca^{2+} levels when $InsP_3Rs$ were directly activated by $InsP_3$ under conditions of RyR blockade. This eventless release is reminiscent of that previously described using a diffusible Ca^{2+} indicator when cardiomyocytes were stimulated with ET-1 or $InsP_3$ (Blanch i Salvador and Egger, 2018; Horn et al., 2013).

The increase in Ca^{2+} nanospark frequency induced by $InsP_3$ uncaging indicates that the numerous other cellular targets of ET-1, including L-type Ca^{2+} channels (He et al., 2000; Lauer et al., 1992; Watanabe and Endoh, 1999), K^+ channels (James et al., 2001), the Na^+/Ca^{2+} exchanger (Yang et al., 1999; Zhang et al., 2006) and the Na^+/H^+ exchanger (Kramer et al., 1991), are not required for ET-1 modulation of dyadic Ca^{2+}. $InsP_3Rs$ may, however, influence cardiomyocyte electrophysiology. Indeed, dyadic localization could allow IICR regulation of the L-type Ca^{2+} current and localization of $InsP_3Rs$ in the neighborhood of the electrogenic Na^+/Ca^{2+} exchanger (NCX; located in microdomains along the TTs that are distinct to release sites), is reported to modulate the electrical properties of ventricular cardiomyocytes that may lead to arrhythmia (Mohler et al., 2005; Signore et al., 2013).

To explain how $InsP_3$ elicits its effects, we reasoned that either Ca^{2+} release via $InsP_3Rs$ served to directly activate RyR clusters or facilitated their activation by Ca^{2+} arising from other sources, including via LTCC and RyRs (Cannell et al., 2013; Kolstad et al., 2018; Walker et al., 2015; Wang et al., 2004; Wescott et al., 2016). The normal cytosolic Ca^{2+} sensitivity of cardiac RyRs is inherently low, resulting in infrequent openings at cytosolic Ca^{2+} concentrations <1 µM (Xu et al., 1996). Modeling studies predict that concentrations of upwards of 10 µM are in fact required for RyR activation indicating that gating of RyRs is only achieved when they are in close vicinity of a Ca^{2+} source (Cannell et al., 2013). Ca^{2+} release via proximal $InsP_3Rs$ could therefore act via CICR to stimulate RyR openings. Furthermore, based on the notion that clusters rapidly shut down when RyRs numbers are low or are disorganized, IICR could also act to maintain cluster activity and increase spark fidelity (Walker et al., 2015).

Journal of Cell Science (2021) 135, jcs258671. doi:10.1242/jcs.258671

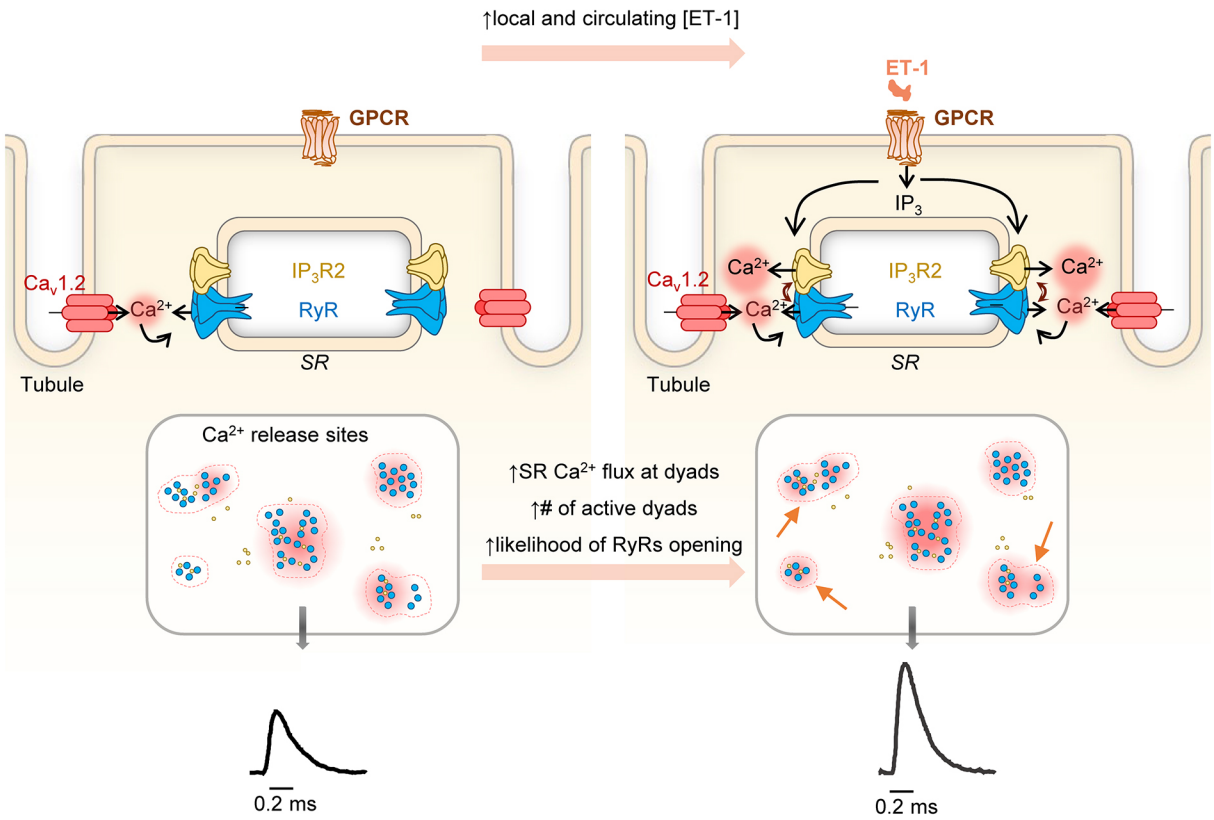

Fig. 7. Illustration of the mechanism by which ET-1 via activation of $InsP_3R$ signaling at the dyad modulates SR Ca^{2+} release during ECC. Following ET-1 stimulation, IICR raises dyadic Ca^{2+} levels, which in turn recruits RyRs during ECC. Through this action, the fidelity of Ca^{2+} spark generation and Ca^{2+} release flux through colocated RyR clusters are increased at single release sites contributing concomitantly to ET-1 modulation of SR Ca^{2+} release during ECC.

Through inducing a leak of Ca^{2+} from the SR, IICR is reported to lead to a reduction in SR Ca^{2+} load (Blanch i Salvador and Egger, 2018). As lower SR Ca^{2+} results in a reduction in RyR-mediated Ca^{2+} release and spark termination (Györke and Györke, 1998), this depletion of the SR Ca^{2+} store could thus lead to a reduction in Ca^{2+} flux during the Ca^{2+} transient. We did not, however, see such an effect of ET-1 activation of IICR under the pacing conditions used for recordings of electrically evoked Ca^{2+} release, suggesting that in healthy cardiomyocytes, homeostatic mechanisms are sufficient to maintain SR Ca^{2+} levels in the face of IICR activation. Further supporting the ability of homeostatic mechanisms to counter substantial Ca^{2+} leak, we also did not see any $InsP_3$-stimulated elevation in diastolic Ca^{2+} levels in paced cardiomyocytes or in quiescent cardiomyocytes in which RyRs were inhibited. These findings are in agreement with our previous study (Smyrnias et al., 2018) and are in line with findings in rabbit cardiomyocytes, which showed a substantially lower Ca^{2+} leak via $InsP_3Rs$ than via RyRs (Zima et al., 2010).

Conclusions

Through activation of dyadic $InsP_3R$-dependent Ca^{2+} signaling to RyRs and a consequent increase in the fidelity of Ca^{2+} spark generation, ET-1, and possibly other hormones that act via $G\alpha_q$-coupled GPCRs, modulate SR Ca^{2+} release during ECC in ventricular cardiomyocytes (Fig. 7). Through this recruitment of dyadic RyR clusters and sensitization of the Ca^{2+} release process, ET-1 stimulation augments Ca^{2+} transients and/or promotes an increase in potentially arrhythmogenic extra-systolic Ca^{2+} release events. These effects can be especially detrimental under the circumstances of RyR post-translational modifications, such as by Ca^{2+}/calmodulin-dependent protein kinase II (CaMKII) and reactive oxygen species (ROS) that sensitize them to Ca^{2+}.

MATERIALS AND METHODS

Ethical statement

All experimental procedures were approved by the in-house ethical committee (Ethische Commissie Dierproeven, KU Leuven), with permit number P070/2018 and comply with European legislation (European Commission Directive 2010/63/EU) on animal care.

Adult rat ventricular cardiomyocyte isolation, culture and adenoviral infection

Cardiomyocytes were enzymatically isolated from male 6–7-week-old Wistar Kyoto rats (weight 180–210 g) purchased from Harlan Laboratories (Horst, The Netherlands). Briefly, rats were deeply anesthetized by intraperitoneal injection of pentobarbital (80 mg/kg body weight) supplemented with heparin (2500 units/kg body weight) in the same syringe to prevent blood coagulation, and subsequently killed by cervical dislocation. The heart was removed from the rat via bilateral thoracotomy, placed on a Langendorff perfusion apparatus and digested with collagenase II (Worthington Biochemical Corp., Lakewood, HJ, USA) at 37°C as previously described (Smyrnias et al., 2018). Culture and viral infections were performed with modifications from that previously described (Drawnel et al., 2012). Freshly isolated cardiomyocytes were plated on 18 mm coverslips coated with 25 µg/ml laminin (Gibco, #23017015) and thereafter cultured in M199 medium (Sigma-Aldrich, #M7528), supplemented with 0.1% bovine serum albumin (BSA), 1% insulin-transferrin-selenium and penicillin/streptomycin, 5 mM creatine, 2 mM L-carnitine, 5 mM taurine. At 1 hour after plating, unattached cells were removed and remaining cardiomyocytes were infected with adenovirus carrying the target gene at a multiplicity of infection of 100. Cardiomyocytes were used for

experiments after 48 h in culture. Cardiomyocytes that responded to electrical stimulation and did not show spontaneous activity were selected for analysis (Fig. S1A).

Molecular biology and preparation of adenoviruses

The recombinant adenoviral plasmid that contained GCaMP6f–triadin gene was kindly provided by Prof. Heping Cheng (Peking University, China; Shang et al., 2014). pGP-CMV-GCaMP6f was from Addgene (#40755; deposited by Douglas S. Kim; Chen et al., 2013). Adenoviruses were generated using the AdEasy Adenoviral vector system (Agilent Technologies, #240009). Briefly, the coding region of the gene to be expressed was cloned into the pShuttle-CMV vector, after which it was recombined into pAdEasy-1 vector by LR recombinase reaction in *E. coli*. After sequence-verification the adenoviral recombinant plasmid was linearized with PacI and, after purification with SureClean Plus beads (Bioline, #BIO-37047), was transfected into HEK293 cells (Microbix Biosystems Inc., Ontario, Canada). Crude adenovirus was harvested after 10–14 days. This crude viral preparation was used for large-scale amplification of virus in HEK293 cells, which was purified using the Vivapure AdenoPack 100 RT kit (Sartorius, #VS-AVPQ102). Adenoviral stock titer was determined using an end-point dilution assay.

Confocal Ca^{2+} imaging

On the day of experiment, coverslips were mounted in the imaging chamber (Multichannel systems; model #RC-49MFSH), supplemented with perfusion and aspiration system, and a solenoid-controlled local perfusion system was positioned near the cell to allow continuous perfusion and rapid switching between control and agonist or blocker solutions. Throughout the experiment, cells were constantly perfused with normal Tyrode solution (135 mM NaCl, 5.4 mM KCl, 10 mM HEPES, 10 mM D-glucose, 2 mM $MgCl_2$ and 1 mM $CaCl_2$ at pH 7.35). All experiments were performed at room temperature on cardiomyocytes electrically paced with a pair of platinum electrodes at a stimulation frequency of 0.5 Hz. A voltage was set at the value required to evoke contraction in >90% of cardiomyocytes. To visualize TTs, cardiomyocyte membranes were fluorescently labeled with Di-8-ANEPPS (Thermo Fisher Scientific, #D3167; 5 µM) dye for 5 min. Ca^{2+} imaging was performed using a Nikon A1R confocal microscope through a Nikon Apo 60× Oil λS DIC N2 (1.4 NA) oil immersion objective, the pinhole was set to 1 A.U. achieving a Z-section thickness of 0.42 µm. Ca^{2+} transients were recorded at 512 lines/s with a pixel size of 0.19–0.22 µm.

Reagents

Pharmacological agents were from Sigma-Aldrich (Belgium) and concentrations used were as follows: isoproterenol, 10 nM (Iso; #I6504); endothelin-1, 100 nM (ET-1; #E7764); angiotensin II, 1 µM (Ang II; #A9525); 2-aminoethyl diphenylborinate, 2 µM (2-APB; #D9754); tetracaine, 1 mM (#T7508); caffeine, 20 mM (#C0750); $InsP_3$ AM, 1 µM (cag-$InsP_3$; SiChem GmbH, #cag-iso-2-145-1).

Ca^{2+} release measurements and protocols

Local and spatially averaged SR Ca^{2+} release signals were measured using GCaMP6f–triadin (GCaMP6f-T) and non-targeted GCaMP6f. For analysis of dyadic Ca^{2+} release during Ca^{2+} transients, cardiomyocytes were paced at 0.5 Hz. At the end of the experiment, to determine the SR Ca^{2+} load and all recruitable Ca^{2+} release sites, electrical stimulation was stopped and 20 mM caffeine rapidly applied. To measure the effect of treatment on the frequency and properties of elementary Ca^{2+} release events, pacing was paused for 30 s to record spontaneous Ca^{2+} release events. For experiments involving photo-release of $InsP_3$, cardiomyocytes were loaded with cag-$InsP_3$ diluted to 1 µM in Pluronic F-127 (Thermo Fisher Scientific, #P30000MP) for 1 h. $InsP_3$ was photo-released at user-defined cellular regions using the 405 nm laser integrated in the Nikon A1R confocal imaging system. The laser exposure required to achieve uncaging was determined empirically by imaging Ca^{2+} release in HeLa cells, which express $InsP_3$Rs. Four exposures of 250 ms duration (pixel dwell time is 7.5 µs) with the laser at 100% was found to achieve optimal uncaging.

Image analysis

Analysis of local cytosolic Ca^{2+} release and elementary Ca^{2+} release events was performed using Fiji (Schindelin et al., 2012) and Matlab (The MathWorks Inc., Natick, MA). Acquired fluorescence linescan images were processed using custom-written routines in ImageJ (available from the authors upon request). Parameters of Ca^{2+} signals were calculated from the extracted profiles of fluorescence change using Matlab. The amplitude and maximal rate of SR Ca^{2+} release of spatially averaged Ca^{2+} transients were analyzed after normalization to resting fluorescence levels (F/F_0) in Matlab. The time course of fluorescence was averaged for 5 pixels around the center of the identified release site. Synchrony of Ca^{2+} release was assessed as previously described (Song et al., 2001), by measuring the latency of Ca^{2+} release onset in relation to the earliest release site and measuring the standard deviation of these values. The peak of the first derivative of fluorescence change [max(ΔF_0/ms)] during Ca^{2+} release was used as a measure of maximal Ca^{2+} release flux from the SR as previously described (Sipido and Wier, 1991). Only active release sites that displayed a fluorescence change exceeding the threshold of 5×SD×F_0 were included in the analysis. For each release site, kinetic parameters of Ca^{2+} release were averaged from the seven consecutive Ca^{2+} transients to reduce the effect of beat-to-beat variability of stochastic Ca^{2+} release via RyRs. SR Ca^{2+} content was assessed by rapidly applying 20 mM caffeine and measuring the amplitude of the elicited Ca^{2+} transient.

The SparkMaster plugin implemented in ImageJ was used to analyze Ca^{2+} spark parameters (Picht et al., 2007). The Ca^{2+} spark event detection was set at six times the standard deviation of the background noise over the mean value of the background. This value was required to accommodate for the non-homogeneous distribution of targeted GCaMP6f. Detected events were further verified by manual analysis. Parameters analyzed included spark frequency (normalized to cell length and time), amplitude ($\Delta F/F_0$), size (full width at half-maximal amplitude; FWHM), duration (full duration at half-maximal amplitude; FDHM), rise time (time to peak; TTP) and maximal Ca^{2+} release rate [max(ΔF_0/ms)]. Ca^{2+} spark mass was calculated according to the formula $1.206\times\Delta F/F_0\times FWHM^3$ (Chandler et al., 2003). Spark-mediated Ca^{2+} leak was calculated as the product of spark mass and frequency.

Immunofluorescence and imaging

Cardiomyocytes expressing GCaMP6f–triadin were fixed with 1% paraformaldehyde (PFA) in normal Tyrode solution for 5 min at room temperature. The distribution of GCaMP6f–triadin relative to SR Ca^{2+} release channels was investigated by confocal microscopy. In brief, dual labeling was performed using rabbit anti-RyR2 (gift from Prof. V. Sorrentino, University of Sienna; 1:200; Giannini et al., 1995) or anti-$InsP_3$R2 (Atlas Antibodies, HPA059144; Lot#R82918; 1:100) primary antibodies in combination with a cocktail of mouse anti-NCX1 (Swant, R3F1; Lot#mr05; 1:200) and anti-caveolin-3 (BD Bioscience, N610420; 1:200) primary antibodies designed to stain the sarcolemma and TTs as previously described (Hou et al., 2015; Munro et al., 2016). For simultaneous visualization of $InsP_3$Rs and RyRs, dual labeling was performed with mouse anti-RyR1 (clone 34C, which also recognizes type 2 RyR) (Invitrogen, #MA3-925; Lot#TG268734; 1:200) and rabbit anti-$InsP_3$R2 (Atlas Antibodies, HPA059144; 1:100) primary antibodies. Cardiomyocytes were permeabilized with PBS containing 0.4% Triton X-100 (diluted from Surfact-Amps detergent solution, Thermo Fisher Scientific, #28314) for 15 min at room temperature, followed by blocking with either 5% normal goat serum (NGS) (Sigma-Aldrich, #S26-M) in PBS (for RyR2 antibody) or Image-iT Signal Enhancer ($InsP_3$R antibody; Thermo Fisher Scientific, #I36933) for 1 h at room temperature. Primary antibodies were applied overnight at 4°C in a buffer composed of PBS, 0.1% Triton X-100, 2% BSA and 2% NGS. Appropriate secondary antibodies, conjugated to either Alexa Fluor 568 (goat anti-rabbit, Thermo Fisher Scientific, # A-11036) or Alexa Fluor 647 (goat anti-mouse, Thermo Fisher Scientific, # A-21236), were applied at a dilution of 1:100 or 1:500 for goat anti-rabbit-IgG and 1:200 for goat anti-mouse-IgG to stain $InsP_3$R2, RyR2 and TTs/sarcolemma, respectively. All secondary antibodies were incubated for 2 h at room temperature. Cardiomyocytes were mounted on glass slides in Vectashield containing DAPI (Vector Laboratories, #H-1200-10), and images were acquired using a Nikon A1R confocal microscope configured

on a Nikon Ti2 equipped with a Nikon Apo 60×/1.4 NA (MRD71600) oil immersion objective. The pinhole was set to achieve a *Z*-section thickness of 0.45 µm. Images were acquired with voxel size set at 0.11×0.11×0.2 µm.

Acquired image stacks were deconvolved using Huygens Professional version 19.04 (Scientific Volume Imaging, The Netherlands), using the CMLE algorithm with the signal to noise ratio set at 20 and iterations to 40. A single image of the stack from the cell central plane was used to assess relative expression of proteins. After images for each protein staining were thresholded, the relative distances were measured using a custom-written macro in ImageJ and were calculated as Euclidean distance between the center of two nearest clusters. Additionally, overlap between two proteins of interest was calculated in analogy with Manders' coefficient.

GCaMP6f–triadin expression analysis of confocal images

Quantitative analysis of cellular GCaMP6f–triadin protein expression relative to RyRs and TTs was based on confocal immunofluorescence imaging as described above. To exclude sub-sarcolemmal cellular regions of the analysis, the cell mask was created by blurring the RyR2 images (Gaussian Blur, sigma 25 pixels) and consecutive dilation (25 pixels). Similarly, nuclei and perinuclear regions were removed from GCaMP6f–triadin, TT and RyR2 images. To create a mask of these regions, DAPI images were consecutively smoothed (mean, radius 1 pixel), blurred (Gaussian Blur, sigma 15 pixels) and binarized. The immunofluorescence signal pattern of GCaMP6f–triadin, TTs and RyR2 was segmented with Fiji operations: (1) GCaMP6f–traidin images were background subtracted (rolling ball radius: 5 pixels), smoothed (mean, radius 2 pixels), and global Moments thresholding was used to binarize the GCaMP6f-triadin signals; (2) TT images were smoothed (median, radius 2 pixels), segmented by local Bernsen thresholding (radius: 15) and consecutively skeletonized; and (3) RyR2 images were background subtracted (rolling ball radius: 5 pixels), smoothed (median, radius 2 pixels) and segmented by local Otsu thresholding (radius: 12). Watershed function was applied to separate adjacent clusters that were segmented together. Binarized images were then used to determine the percentage of GCaMP6f–triadin clusters overlapping with RyR2 signals and TTs. For overlap analysis, we accepted clusters that ranged between partial and mutually complete overlap in binarized images. The skeleton of TTs was used to calculate the Euclidean distance between TTs and GCaMP6f–triadin clusters.

$InsP_3R$ expression analysis of confocal images

Quantitative analysis of cellular expression of $InsP_3Rs$ was performed as described for GCaMP6f–triadin except for image processing and segmentation methods, which were as follows: (1) RyR2 images were background subtracted (rolling ball radius: 10), smoothed (mean, radius 1 pixel) and segmented by local Bernsen thresholding (radius: 5); (2) $InsP_3R2$ images were background subtracted (rolling ball radius: 15), smoothed (median, radius 1 pixel) and binarized by local Otsu threshold (radius: 15); and (3) TT images were smoothed (median, 1 pixel), segmented by local Otsu threshold (radius: 18) and consequently skeletonized.

Statistical analysis

All individual data points are shown in dot plots, with each dot representing a cell. Normal distribution of data was assessed with D'Agostino & Pearson omnibus normality testing (α=0.05). Data is reported as mean±s.e.m, Tukey boxplots (median with whiskers equaling 1.5 times the interquartile range), mean±s.d., or as before-and-after measurements, and the calculated effect sizes (Δ) with 95% confidence interval. Statistical comparisons were made using paired or unpaired Student's *t*-test, Wilcoxon matched-pairs signed rank test (paired data, non-normal distribution), Mann–Whitney U (unpaired data, non-normal distribution) and ordinary one-way ANOVA with Bonferroni post hoc test to compare more than two groups. A repeated measures two-way ANOVA test with Bonferroni post hoc testing was applied for pharmacological interventions. Difference in distributions of maximal dyadic Ca^{2+} release fluxes and Ca^{2+} sparks parameters was assessed using an equal variance (F) test. Statistical analysis was performed using GraphPad Prism 9 software (GraphPad Software, La Jolla, California, USA) and statistical significance was set at $P<0.05$. The number of animals ($N_{animals}$), cells (n_{cells}), release sites ($n_{release\ sites}$) and Ca^{2+} release events are given in the figure legends. Sample sizes were determined by power analysis based on data in our previous publication on similar parameters (Harzheim et al., 2009). We assessed the presence of outliers by using ROUT method implemented in Graphpad (with Q=1%).

Acknowledgements

We thank Roxane Menten for assistance with animal handling and cell isolation, Prof. Heping Cheng for the GCaMP6f-triadin construct and Prof. Douglas S. Kim & Genie project (Howard Hughes Medical Institute, USA) for the pGP-CMV-GCaMP6f plasmid. RyR2 antibody was a gift from Prof. Vincenzo Sorrentino (University of Siena, Italy).

Competing interests

The authors declare no competing or financial interests.

Author contributions

Conceptualization: H.L.R.; Methodology: K.D., K.R.S., H.L.R.; Formal analysis: K.D., H.L.R.; Investigation: K.D., H.L.R.; Resources: K.R.S., H.L.R.; Data curation: K.D., H.L.R.; Writing - original draft: K.D., H.L.R.; Writing - review & editing: K.D., K.R.S., H.L.R.; Visualization: K.D., H.L.R.; Supervision: H.L.R.; Project administration: H.L.R.; Funding acquisition: H.L.R.

Funding

This work was supported by the KU Leuven and the Fund for Scientific Research-Flanders [Fonds Wetenschappelijk Onderzoek (FWO) project grant (G08861N, Odysseus Project 90663 to H.L.R.)].

References

Acsai, K., Antoons, G., Livshitz, L., Rudy, Y. and Sipido, K. R. (2011). Microdomain [Ca^{2+}] near ryanodine receptors as reported by L-type Ca^{2+} and Na^+/Ca^{2+} exchange currents. *J. Physiol.* **589**, 2569-2583. doi:10.1113/jphysiol.2010.202663

Bare, D. J., Kettlun, C. S., Liang, M., Bers, D. M. and Mignery, G. A. (2005). Cardiac type 2 inositol 1,4,5-trisphosphate receptor: Interaction and modulation by calcium/calmodulin-dependent protein kinase II. *J. Biol. Chem.* **280**, 15912-15920. doi:10.1074/jbc.M414212200

Bers, D. M. (2002). Cardiac excitation-contraction coupling. *Nature* **415**, 198-205. doi:10.1038/415198a

Blanch i Salvador, J. and Egger, M. (2018). Obstruction of ventricular Ca^{2+}-dependent arrhythmogenicity by inositol 1,4,5-trisphosphate-triggered sarcoplasmic reticulum Ca^{2+} release. *J. Physiol.* **596**, 4323-4340. doi:10.1113/JP276319

Brette, F. and Orchard, C. (2003). T-tubule function in mammalian cardiac myocytes. *Circ. Res.* **92**, 1182-1192. doi:10.1161/01.RES.0000074908.17214.FD

Cannell, M. B., Kong, C. H. T., Imtiaz, M. S. and Laver, D. R. (2013). Control of sarcoplasmic reticulum Ca^{2+} release by stochastic RyR gating within a 3D model of the cardiac dyad and importance of induction decay for CICR termination. *Biophys. J.* **104**, 2149-2159. doi:10.1016/j.bpj.2013.03.058

Chandler, W. K., Hollingworth, S. and Baylor, S. M. (2003). Simulation of calcium sparks in cut skeletal muscle fibers of the frog. *J. Gen. Physiol.* **121**, 311-324. doi:10.1085/jgp.200308787

Chen, T. W., Wardill, T. J., Sun, Y., Pulver, S. R., Renninger, S. L., Baohan, A., Schreiter, E. R., Kerr, R. A., Orger, M. B., Jayaraman, V. et al. (2013). Ultrasensitive fluorescent proteins for imaging neuronal activity. *Nature* **499**, 295-300. doi:10.1038/nature12354

Despa, S., Shui, B., Bossuyt, J., Lang, D., Kotlikoff, M. I. and Bers, D. M. (2014). Junctional cleft $[Ca^{2+}]_i$ measurements using novel cleft-targeted Ca^{2+} sensors. *Circ. Res.* **115**, 339-347. doi:10.1161/CIRCRESAHA.115.303582

Dickinson, G. D., Swaminathan, D. and Parker, I. (2012). The probability of triggering calcium puffs is linearly related to the number of inositol trisphosphate receptors in a cluster. *Biophys. J.* **102**, 1826-1836. doi:10.1016/j.bpj.2012.03.029

Domeier, T. L., Zima, A. V., Maxwell, J. T., Huke, S., Mignery, G. A. and Blatter, L. A. (2008). IP_3 receptor-dependent $Ca2^+$ release modulates excitation-contraction coupling in rabbit ventricular myocytes. *Am. J. Physiol. Heart Circ. Physiol.* **294**, H596-H604. doi:10.1152/ajpheart.01155.2007

Drawnel, F. M., Wachten, D., Molkentin, J. D., Maillet, M., Aronsen, J. M., Swift, F., Sjaastad, I., Liu, N., Catalucci, D., Mikoshiba, K. et al. (2012). Mutual antagonism between IP_3RII and miRNA-133a regulates calcium signals and cardiac hypertrophy. *J. Cell Biol.* **199**, 783-798. doi:10.1083/jcb.201111095

Drawnel, F. M., Archer, C. R. and Roderick, H. L. (2013). The role of the paracrine/autocrine mediator endothelin-1 in regulation of cardiac contractility and growth. *Br. J. Pharmacol.* **168**, 296-317. doi:10.1111/j.1476-5381.2012.02195.x

Dries, E., Bito, V., Lenaerts, I., Antoons, G., Sipido, K. R. and Macquaide, N. (2013). Selective modulation of coupled ryanodine receptors during microdomain activation of calcium/calmodulin-dependent kinase II in the dyadic cleft. *Circ. Res.* **113**, 1242-1252. doi:10.1161/CIRCRESAHA.113.301896

Foskett, J. K., White, C., Cheung, K.-H. and Mak, D.-O. D. (2007). Inositol trisphosphate receptor Ca^{2+} release channels. *Physiol. Rev.* **87**, 593-658. doi:10.1152/physrev.00035.2006

Galice, S., Xie, Y., Yang, Y., Sato, D. and Bers, D. M. (2018). Size matters: ryanodine receptor cluster size affects arrhythmogenic sarcoplasmic reticulum calcium release. *J. Am. Heart Assoc.* **7**, e008724. doi:10.1161/JAHA.118.008724

Giannini, G., Conti, A., Mammarella, S., Scrobogna, M. and Sorrentino, V. (1995). The ryanodine receptor/calcium channel genes are widely and differentially expressed in murine brain and peripheral tissues. *J. Cell Biol.* **128**, 893-904. doi:10.1083/jcb.128.5.893

Gilbert, G., Demydenko, K., Dries, E., Puerta, R. D., Xin, J., Sipido, K. and Roderick, H. L. (2020). Calcium signalling in cardiomyocyte function. *Cold Spring Harb. Perspect Biol.* **12**, a035428. doi:10.1101/cshperspect.a035428

Go, L. O., Moschella, M. C., Watras, J., Handa, K. K., Fyfe, B. S. and Marks, A. R. (1995). Differential regulation of two types of intracellular calcium release channels during end-stage heart failure. *J. Clin. Invest.* **95**, 888-894. doi:10.1172/JCI117739

Gwathmey, J. K., Hajar, R. J. and Solaro, R. J. (1991). Contractile deactivation and uncoupling of crossbridges. Effects of 2,3–butanedione monoxime on mammalian myocardium. *Circ. Res.* **69**, 1280-1292. doi:10.1161/01.res.69.5.1280

Györke, I. and Györke, S. (1998). Regulation of the cardiac ryanodine receptor channel by luminal Ca^{2+} involves luminal Ca^{2+} sensing sites. *Biophys. J.* **75**, 2801-2810. doi:10.1016/S0006-3495(98)77723-9

Harzheim, D., Movassagh, M., Foo, R. S.-Y., Ritter, O., Tashfeen, A., Conway, S. J., Bootman, M. D. and Roderick, H. L. (2009). Increased $InsP_3Rs$ in the junctional sarcoplasmic reticulum augment Ca^{2+} transients and arrhythmias associated with cardiac hypertrophy. *Proc. Natl. Acad. Sci. USA* **106**, 11406-11411. doi:10.1073/pnas.0905485106

Harzheim, D., Talasila, A., Movassagh, M., Foo, R. S. Y., Figg, N., Bootman, M. D. and Roderick, H. L. (2010). Elevated $InsP_3R$ expression underlies enhanced calcium fluxes and spontaneous extra-systolic calcium release events in hypertrophic cardiac myocytes. *Channels* **4**, 67-71. doi:10.4161/chan.4.1.11537

He, J. Q., Pi, Y. Q., Walker, J. W. and Kamp, T. J. (2000). Endothelin-1 and photoreleased diacylglycerol increase L-type Ca^{2+} current by activation of protein kinase C in rat ventricular myocytes. *J. Physiol.* **524**, 807-820. doi:10.1111/j.1469-7793.2000.00807.x

Helassa, N., Podor, B., Fine, A. and Török, K. (2016). Design and mechanistic insight into ultrafast calcium indicators for monitoring intracellular calcium dynamics. *Sci. Rep.* **6**, 28276. doi:10.1038/srep38276

Hiroe, M., Hirata, Y., Fujita, N., Umezawa, S., Ito, H., Tsujino, M., Koike, A., Nogami, A., Takamoto, T. and Marumo, F. (1991). Plasma endothelin-1 levels in idiopathic dilated cardiomyopathy. *Am. J. Cardiol.* **68**, 1114-1115. doi:10.1016/0002-9149(91)90511-I

Horn, T., Ullrich, N. D. and Egger, M. (2013). "Eventless" $InsP_3$-dependent SR-Ca^{2+} release affecting atrial Ca^{2+} sparks. *J. Physiol.* **591**, 2103-2111. doi:10.1113/jphysiol.2012.247288

Hou, Y., Jayasinghe, I., Crossman, D. J., Baddeley, D. and Soeller, C. (2015). Nanoscale analysis of ryanodine receptor clusters in dyadic couplings of rat cardiac myocytes. *J. Mol. Cell. Cardiol.* **80**, 45-55. doi:10.1016/j.yjmcc.2014.12.013

James, A. F., Ramsey, J. E., Reynolds, A. M., Hendry, B. M. and Shattock, M. J. (2001). Effects of endothelin-1 on K^+ currents from rat ventricular myocytes. *Biochem. Biophys. Res. Commun.* **284**, 1048-1055. doi:10.1006/bbrc.2001.5083

Kolega, J. (2004). Phototoxicity and photoinactivation of blebbistatin in UV and visible light. *Biochem. Biophys. Res. Commun.* **320**, 1020-1025. doi:10.1016/j.bbrc.2004.06.045

Kolstad, T. R., van den Brink, J., Macquaide, N., Lunde, P. K., Frisk, M., Aronsen, J. M., Norden, E. S., Cataliotti, A., Sjaastad, I., Sejersted, O. M. et al. (2018). Ryanodine receptor dispersion disrupts Ca 2+ release in failing cardiac myocytes. *Elife* **7**, 1-24. doi:10.7554/eLife.39427

Kramer, B. K., Smith, T. W. and Kelly, R. A. (1991). Endothelin and increased contractility in adult rat ventricular myocytes. Role of intracellular alkalosis induced by activation of the protein kinase C-dependent Na^+-H^+ exchanger. *Circ. Res.* **68**, 269-279. doi:10.1161/01.RES.68.1.269

Lauer, M. R., Gunn, M. D. and Clusin, W. T. (1992). Endothelin activates voltage-dependent Ca^{2+} current by a G protein-dependent mechanism in rabbit cardiac myocytes. *J. Physiol.* **448**, 729-747. doi:10.1113/jphysiol.1992.sp019067

Ljubojevic, S., Radulovic, S., Leitinger, G., Sedej, S., Sacherer, M., Holzer, M., Winkler, C., Pritz, E., Mittler, T., Schmidt, A. et al. (2014). Early remodelling of perinuclear Ca^{2+} stores and nucleoplasmic Ca^{2+} signalling during the development of hypertrophy and heart failure. *Circulation* **130**, 244-255. doi:10.1161/CIRCULATIONAHA.114.008927

Mayourian, J., Ceholski, D. K., Gonzalez, D. M., Cashman, T. J., Sahoo, S., Hajar, R. J. and Costa, K. D. (2018). Physiologic, pathologic, and therapeutic paracrine modulation of cardiac excitation-contraction coupling. *Circ. Res.* **122**, 167-183. doi:10.1161/CIRCRESAHA.117.311589

McMurray, J. J., Ray, S. G., Abdullah, I., Dargie, H. J. and Morton, J. J. (1992). Plasma endothelin in chronic heart failure. *Circulation* **85**, 1374-1379. doi:10.1161/01.CIR.85.4.1374

Mohler, P. J., Davis, J. Q. and Bennett, V. (2005). Ankyrin-B coordinates the Na/K ATPase, Na/Ca exchanger, and $InsP_3$ receptor in a cardiac T-tubule/SR microdomain. *PLoS Biol.* **3**, e423. doi:10.1371/journal.pbio.0030423

Munro, M. L., Jayasinghe, I. D., Wang, Q., Quick, A., Wang, W., Baddeley, D., Wehrens, X. H. T. and Soeller, C. (2016). Junctophilin-2 in the nanoscale organisation and functional signalling of ryanodine receptor clusters in cardiomyocytes. *J. Cell Sci.* **129**, 4388-4398. doi:10.1242/jcs.196873

Nakayama, H., Bodi, I., Maillet, M., DeSantiago, J., Domeier, T. L., Mikoshiba, K., Lorenz, J. N., Blatter, L. A., Bers, D. M. and Molkentin, J. D. (2010). The IP_3 receptor regulates cardiac hypertrophy in response to select stimuli. *Circ. Res.* **107**, 659-666. doi:10.1161/CIRCRESAHA.110.220038

Peppiatt, C. M., Collins, T. J., Mackenzie, L., Conway, S. J., Holmes, A. B., Bootman, M. D., Berridge, M. J., Seo, J. T. and Roderick, H. L. (2003). 2–Aminoethoxydiphenyl borate (2-APB) antagonises inositol 1,4,5-trisphosphate-induced calcium release, inhibits calcium pumps and has a use-dependent and slowly reversible action on store-operated calcium entry channels. *Cell Calcium* **34**, 97-108. doi:10.1016/S0143-4160(03)00026-5

Picht, E., Zima A, V., Blatter, L. A. and Bers, D. M. (2007). SparkMaster: automated calcium spark analysis with ImageJ. *Am. J. Physiol. Cell Physiol.* **293**, 1073-1081. doi:10.1152/ajpcell.00586.2006.-Ca

Picht, E., Zima A, V., Shannon, T. R., Duncan, A. M., Blatter, L. A. and Bers, D. M. (2011). Dynamic calcium movement inside cardiac sarcoplasmic reticulum during release. *Circ. Res.* **108**, 847-856. doi:10.1161/CIRCRESAHA.111.240234

Proven, A., Roderick, H. L., Conway, S. J., Berridge, M. J., Horton, J. K., Capper, S. J. and Bootman, M. D. (2006). Inositol 1,4,5–trisphosphate supports the arrhythmogenic action of endothelin-1 on ventricular cardiac myocytes. *J. Cell Sci.* **119**, 3363-3375. doi:10.1242/jcs.03073

Regitz-Zagrosek, V., Friedel, N., Heymann, A., Bauer, P., Neuß, M., Rolfs, A., Steffen, C., Hildebrandt, A., Hetzer, R. and Fleck, E. (1995). Regulation, chamber localization, and subtype distribution of angiotensin II receptors in human hearts. *Circulation* **91**, 1461-1471. doi:10.1161/01.CIR.91.5.1461

Schindelin, J., Arganda-Carreras, I., Frise, E., Kaynig, V., Longair, M., Pietzsch, T., Preibisch, S., Rueden, C., Saalfeld, S., Schmid, B. et al. (2012). Fiji: an open-source platform for biological-image analysis. *Nat. Methods* **9**, 676-682. doi:10.1038/nmeth.2019

Shang, W., Lu, F., Sun, T., Xu, J., Li, L.-L., Wang, Y., Wang, G., Chen, L., Wang, X., Cannell, M. B. et al. (2014). Imaging Ca^{2+} nanosparks in heart with a new targeted biosensor. *Circ. Res.* **114**, 412-420. doi:10.1161/CIRCRESAHA.114.302938

Shannon, T. R., Wang, F., Puglisi, J., Weber, C. and Bers, D. M. (2004). A mathematical treatment of integrated Ca dynamics within the ventricular myocyte. *Biophys. J.* **87**, 3351-3371. doi:10.1529/biophysj.104.047449

Signore, S., Sorrentino, A., Ferreira-Martins, J., Kannappan, R., Shafaie, M., Del Ben, F., Isobe, K., Arranto, C., Wybieralska, E., Webster, A. et al. (2013). Inositol 1, 4, 5–trisphosphate receptors and human left ventricular myocytes. *Circulation* **128**, 1286-1297. doi:10.1161/CIRCULATIONAHA.113.002764

Sipido, K. R. and Wier, W. G. (1991). Flux of Ca^{2+} across the sarcoplasmic reticulum of guinea-pig cardiac cells during excitation-contraction coupling. *J. Physiol.* **435**, 605-630. doi:10.1113/jphysiol.1991.sp018528

Smith, G. L., Valdeolmillos, M., Eisner, D. A. and Allen, D. G. (1988). Effects of rapid application of caffeine on intracellular calcium concentration in ferret papillary muscles. *J. Gen. Physiol.* **92**, 351-368. doi:10.1085/jgp.92.3.351

Smyrnias, I., Goodwin, N., Wachten, D., Skogestad, J., Aronsen, J. M., Robinson, E. L., Demydenko, K., Segonds-Pichon, A., Oxley, D., Sadayappan, S. et al. (2018). Contractile responses to endothelin-1 are regulated by PKC phosphorylation of cardiac myosin binding protein-C in rat ventricular myocytes. *J. Mol. Cell. Cardiol.* **17**, 1-18. doi:10.1016/j.yjmcc.2018.02.012

Song, L.-S., Sham, J. S. K., Stern, M. D., Lakatta, E. G. and Cheng, H. (1998). Direct measurement of SR release flux by tracking "Ca^{2+} spikes" in rat cardiac myocytes. *J. Physiol.* **512**, 677-691. doi:10.1111/j.1469-7793.1998.677bd.x

Song, L.-S., Wang, S.-Q., Xiao, R.-P., Spurgeon, H., Lakatta, E. G. and Cheng, H. (2001). B-Adrenergic stimulation synchronizes intracellular Ca^{2+} release during excitation-contraction coupling in cardiac myocytes. *Circ. Res.* **88**, 794-801. doi:10.1161/hh0801.090461

Stewart, D. J., Cernacek, P., Costello, K. B. and Rouleau, J. L. (1992). Elevated endothelin-1 in heart failure and loss of normal response to postural change. *Circulation* **85**, 510-517. doi:10.1161/01.CIR.85.2.510

Sun, X.-H., Protasi, F., Takahashi, M., Takeshima, H., Ferguson, D. G. and Franzini-Armstrong, C. (1995). Molecular architecture of membranes involved in excitation-contraction coupling of cardiac muscle. *J. Cell Biol.* **129**, 659-671. doi:10.1083/jcb.129.3.659

Tsutsumi, Y., Matsubara, H., Ohkubo, N., Mori, Y., Nozawa, Y., Murasawa, S., Kijima, K., Maruyama, K., Masaki, H., Moriguchi, Y. et al. (1998). Angiotensin II type 2 receptor is upregulated in human heart with interstitial fibrosis, and cardiac fibroblasts are the major cell type for its expression. *Circ. Res.* **83**, 1035-1046. doi:10.1161/01.RES.83.10.1035

Van De Wal, R. M. A., Plokker, H. W. M., Lok, D. J. A., Boomsma, F., van der Horst, F. A. L., van Veldhuisen, D. J., van Gilst, W. H. and Voors, A. A. (2006). Determinants of increased angiotensin II levels in severe chronic heart failure

patients despite ACE inhibition. *Int. J. Cardiol.* **106**, 367-372. doi:10.1016/j.ijcard.2005.02.016

Walker, M. A., Kohl, T., Lehnart, S. E., Greenstein, J. L., Lederer, W. J. and Winslow, R. L. (2015). On the adjacency matrix of RyR2 cluster structures. *PLoS Comput. Biol.* **11**, e1004521. doi:10.1371/journal.pcbi.1004521

Wang, S. Q., Stern, M. D., Ríos, E. and Cheng, H. (2004). The quantal nature of Ca^{2+} sparks and in situ operation of the ryanodine array cardiac cells. *Proc. Natl. Acad. Sci. USA* **101**, 3979-3984. doi:10.1073/pnas.0306157101

Watanabe, T. and Endoh, M. (1999). Characterization of the endothelin-1-induced regulation of L-type Ca^{2+} current in rabbit ventricular myocytes. *Naunyn Schmiedebergs Arch. Pharmacol.* **360**, 654-664. doi:10.1007/s002109900130

Wescott, A. P., Jafri, M. S., Lederer, W. J. and Williams, G. S. B. (2016). Ryanodine receptor sensitivity governs the stability and synchrony of local calcium release during cardiac excitation-contraction coupling. *J. Mol. Cell. Cardiol.* **92**, 82-92. doi:10.1016/j.yjmcc.2016.01.024

Wu, X., Zhang, T., Bossuyt, J., Li, X., McKinsey, T. A., Dedman, J. R., Olson, E. N., Chen, J., Heller Brown, J. and Bers, D. M. (2006). Local $InsP_3$-dependent perinuclear Ca^{2+} signalling in cardiac myocyte excitation- transcription coupling. *J. Clin. Invest.* **116**, 675-682. doi:10.1172/JCI27374

Wullschleger, M., Blanch, J. and Egger, M. (2017). Functional local crosstalk of inositol 1,4 5- trisphosphate receptor- and ryanodine receptor-dependent Ca^{2+} release in atrial cardiomyocytes. *Cardiovasc. Res.* **113**, 542-552. doi:10.1093/cvr/cvx020

Xu, L., Mann, G. and Meissner, G. (1996). Regulation of cardiac Ca^{2+} release channel (Ryanodine Receptor) by Ca^{2+}, H^+, Mg^{2+}, and adenine nucleotides under normal and simulated ischemic conditions. *Circ. Res.* **79**, 1100-1109. doi:10.1161/01.RES.79.6.1100

Yang, H. T., Sakurai, K., Sugawara, H., Watanabe, T., Norota, I. and Endoh, M. (1999). Role of Na^+/Ca^{2+} exchange in endothelin-1-induced increases in Ca^{2+} transient and contractility in rabbit ventricular myocytes: Pharmacological analysis with KB-R7943. *Br. J. Pharmacol.* **126**, 1785-1795. doi:10.1038/sj.bjp.0702454

Yorikane, R., Sakai, S., Miyauchi, T., Sakurai, T., Sugishita, Y. and Goto, K. (1993). Increased production of endothelin-1 in the hypertrophied rat heart due to pressure overload. *FEBS Lett.* **332**, 31-34. doi:10.1016/0014-5793(93)80476-B

Zhang, Y. H., Hinde, A. K., James, A. F. and Hancox, J. C. (2006). Modulation of the Na^+/Ca^{2+} exchanger by isoprenaline, adenosine, and endothelin-1 in guinea pig ventricular myocytes. *Ann. NY Acad. Sci.* **976**, 535-538. doi:10.1111/j.1749-6632.2002.tb04789.x

Zima A, V. and Blatter, L. A. (2004). Inositol-1,4,5–trisphosphate-dependent Ca^{2+} signalling in cat atrial excitation-contraction coupling and arrhythmias. *J. Physiol.* **555**, 607-615.

Zima, A. V., Bovo, E., Bers, D. M. and , Blatter, L. A. (2010) Ca^{2+} spark-dependent and -independent sarcoplasmic reticulum Ca^{2+} leak in normal and failing rabbit ventricular myocytes. *J. Physiol.* **588**, 4743-4757. doi:10.1113/jphysiol.2010.197913

Zolk, O., Quattek, J., Sitzler, G., Schrader, T., Nickenig, G., Schnabel, P., Shimada, K., Takahashi, M. and Böhm, M. (1999). Expression of endothelin-1, endothelin-converting enzyme, and endothelin receptors in chronic heart failure. *Circulation* **99**, 2118-2123. doi:10.1161/01.CIR.99.16.2118